1.10.3 HMQC / HSQC / HMBC

前述の同種核シフト相関実験と対になっているのが，ここで紹介する異種核シフト相関実験である．先に紹介した HMQC は磁化移動に多量子遷移現象を利用していた．一方，同じく先に紹介した INEPT 法とほぼ同じパルススキームを利用して，一量子遷移を使って磁化移動して相関スペクトルを得ることもできる．それが異種核一量子相関（heteronuclear single quantum coherence spectroscopy，HSQC）である．HMQC と HSQC はいずれも 1-bond ないし 2-bond を隔てた異種核間の相関を測定する方法である．分子量の大きい試料の測定には TROSY[*2]，CRINEPT[*2] などの変法もある．異種核多結合相関（heteronuclear multiple bond connectivity spectroscopy，HMBC）は HMQC の変法であり，delay を長くとることで微小なカップリングをもつ ^{1}H と ^{13}C の相関（しばしば 2-bond ないし 3-bond を隔てる）を測定する方法であり，低分子化合物の構造解析に使われる．なお，これらすべての方法は，まず磁気回転比の大きい ^{1}H の磁化を他核に移して，化学シフトで展開した後，磁化を ^{1}H に戻して観測する手法であり，プローブの項で紹介したインバース測定の実験ということになる．

1.10.4 交差緩和と NOE，NOESY，ROESY[*3]

これまでは，スピンカップリングを介して，言い換えれば化学結合を介して相互作用している核スピンどうしの相関スペクトルを測定する方法を紹介してきた．一方，化学結合を介さなくても，空間的に近接した核スピンどうしは，そのスピン状態により互いの緩和時間に影響を及ぼす（図 1.12）．2 つの核スピンの緩和現象がお互いに影響を及び合うことを交差緩和といい，発見者の名前にちなんで核オーバーハウザー効果（nuclear Overhauser effect，NOE）と呼ぶ．また，NOE による 2 スピン間の相関スペクトルを測定する方法を核オーバーハウザー効果相関分光法（nuclear Overhauser effect spectroscopy，NOESY）と呼ぶ．NOE の強度は理想的な条件下では核間の距離の 6 乗に反比例するため，NOE を正確に測定することで 5 Å 以下の ^{1}H 間の距離情報を得ることができる．

[*2] TROSY（transverse relaxation-optimized spectroscopy：横緩和最適化型相関分光法）および CRINEPT（cross relaxation-enhanced polarization transfer：交差緩和強化型分極移動法）は，いずれも分子量の大きなタンパク質などの観測に適した磁化移動法を用いた相関分光法である．

[*3] ROESY（rotating-frame nuclear Overhauser effect spectroscopy：回転座標系での NOE 相関分光法）は，スピンロックパルスで横磁化に固定された 2 つの核スピンの交差緩和に基づく測定法である．

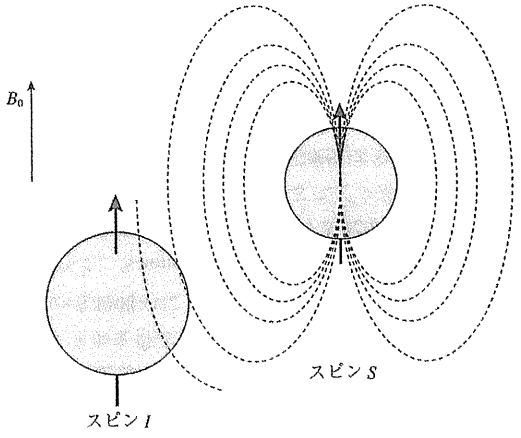

図 1.12 交差緩和と核オーバーハウザー効果
スピン I が感じる磁場はスピン S がつくる磁場の影響を受ける．

1.11 おわりに

以上，なるべく平易な表現で NMR の原理と，NMR を理解するためのいくつかの重要な概念の説明を行った．本章では紙面の都合上駆け足での説明となってしまった．さらに理解を深めるためには，洋書も含めた以下の参考書籍により詳しく学習してほしい．

参考文献

1) 阿久津秀雄，嶋田一夫，鈴木榮一郎，西村善文，日本分光学会測定シリーズ 41：NMR 分光法・原理から応用まで，学会出版センター (2003)
2) 荒田洋治，NMR の書，丸善 (2000)
3) 北丸竜三，核磁気共鳴の基礎と原理，共立出版 (1987)
4) R. Freeman 著，坂口 潮，嶋田一夫，荒田洋治 訳，NMR ハンドブック，共立出版 (1992)
5) 荒田洋治，タンパク質の NMR・構造データの解釈と評価，共立出版 (1996)
6) R. M. Silverstein, F. X. Webster 著，荒木 峻，山本 修，益子洋一郎，鎌田利紘 訳，有機化合物のスペクトルによる同定法―MS，IR，NMR の併用―，東京化学同人 (1999)
7) T. D. W. Claridge 著，竹内敬人，西川実希 訳，有機化学のための高分解能 NMR テクニック，講談社 (2004)
8) H. Kessler, M. Gehrke and C. Griesinger, *Angew. Chem. Int. Ed. Engl.*, **27**, 490 (1988)
9) J. Keeler, *Understanding NMR Spectroscopy*, Wiley-VCH, Weinheim (2005)
10) 黒田義弘，化学と生物実験ライン 16：NMR 実験法―基礎と応用，廣川書店 (1992)
11) R. R. Ernst, G. Bodenhausen, A. Wokaun 著，永山国昭，藤原敏道，内藤 晶，赤坂一之 訳，エルンスト二次元 NMR・原理と測定法（POD 版），吉岡書店 (2000)

THE JOURNAL OF BIOLOGICAL CHEMISTRY VOL. 285, NO. 21, pp. 15931–15940, May 21, 2010

Structure and Mutagenesis Studies of the C-terminal Region of Licensing Factor Cdt1 Enable the Identification of Key Residues for Binding to Replicative Helicase Mcm Proteins

Received for publication, October 18, 2009, and in revised form, March 8, 2010 Published, JBC Papers in Press, March 24, 2010, DOI 10.1074/jbc.M109.075333

JunGoo Jee[‡1,2], Takeshi Mizuno[§1,3], Katsuhiko Kamada[§4], Hidehito Tochio[¶], Yasumasa Chiba[‖], Ken-ichiro Yanagi[§], Gentaro Yasuda[§], Hidekazu Hiroaki[**], Fumio Hanaoka[§‡‡5], and Masahiro Shirakawa[¶]

From the [‡]Center for Priority Areas, Tokyo Metropolitan University, 1-1 Minami-Osawa, Hachioji, Tokyo 192-0397, [§]Cellular Physiology Laboratory, RIKEN Discovery Research Institute, Wako 351-0198, the [¶]Department of Molecular Engineering, Graduate School of Engineering, Kyoto University, Nishikyo, Kyoto 615-8510, [‖]Ajinomoto Company, Kawasaki, Kawasaki 210-8681, the [**]Division of Structural Biology, Graduate School of Medicine, Kobe University, 7-5-1 Kusunoki, Chuo, Kobe, Hyogo 650-0017, and the [‡‡]Faculty of Science, Gakushuin University, 1-5-1 Mejiro, Toshima, Tokyo 171-8588, Japan

In eukaryotes, DNA replication is fired once in a single cell cycle before cell division starts to maintain stability of the genome. This event is tightly controlled by a series of proteins. Cdt1 is one of the licensing factors and is involved in recruiting replicative DNA helicase Mcm2–7 proteins into the pre-replicative complex together with Cdc6. In Cdt1, the C-terminal region serves as a binding site for Mcm2–7 proteins, although the details of these interactions remain largely unknown. Here, we report the structure of the region and the key residues for binding to Mcm proteins. We determined the solution structure of the C-terminal fragment, residues 450–557, of mouse Cdt1 by NMR. The structure consists of a winged-helix domain and shows unexpected similarity to those of the C-terminal domain of Cdc6 and the central fragment of Cdt1, thereby implying functional and evolutionary relationships. Structure-based mutagenesis and an *in vitro* binding assay enabled us to pinpoint the region that interacts with Mcm proteins. Moreover, by performing *in vitro* binding and budding yeast viability experiments, we showed that ~45 residues located in the N-terminal direction of the structural region are equally crucial for recognizing Mcm proteins. Our data suggest the possibility that winged-helix domain plays a role as a common module to interact with replicative helicase in the DNA replication-licensing process.

In eukaryotes, DNA replication is highly coordinated to retain the integrity of the genome. Whereas DNA replication in prokaryotes begins at a single site and stops at the end of the genome, eukaryotic genomes consist of multiple replication origins where DNA replication starts. These origins are synchronized so that they are activated only once in a single division cycle. A series of proteins, the origin recognition complex (ORC),[6] cell division cycle 6 homolog (Cdc6), chromatin licensing and DNA replication factor 1 (Cdt1), and minichromosome maintenance 2–7 (Mcm2–7) are known to play correlated roles in licensing (1–5). Oncogenic proliferation often causes abnormal expression of the proteins involved in the DNA-licensing process, thus emphasizing the importance of harmonious adjustments between these proteins (6). A complicated interaction network between these proteins has been reported (7), although the details at residue and atom levels remain largely unknown.

Formation of a pre-replication complex at each origin is the first event in the replication process. ORC proteins bind initially to each replication origin of DNA. The DNA sequences of the origins where ORC binds have not been identified, except for those in *Saccharomyces cerevisiae* (8), suggesting that there may be other factors involved in addition to the sequences (9). The DNA strand at the origin needs to be unpaired to begin replication; therefore, the existence of replicative helicase is essential. Mcm2–7 proteins are believed to function as the replicative helicase in eukaryotes. Each Mcm2–7 protein consists of a conserved AAA+ ATPase type C-terminal helicase domain and a rather diverse N-terminal domain. The stoichiometry of Mcm2–7 while functioning remains unclear. Both hetero-hexameric and several additional complexes with different combinations of Mcm proteins have been found *in vivo* and *in vitro* (10). Meanwhile, reconstituted Mcm4/6/7 complex has helicase activity *in vitro* (11, 12). The proteins that bridge between ORC and Mcm2–7 are Cdc6 and Cdt1. Cdc6, like Mcm proteins, belongs to the AAA+ ATPase family and shows similarity to clamp loader proteins that load ring-shaped sliding clamps onto DNA (13). The result, Mcm2–7 forming a donut-like ring shape, led to the postulation that Cdc6 behaves as a clamp loader for Mcm2–7 (14, 15).

Cdt1 was originally found in fission yeast (16), and its function as a factor involved in replication licensing was first characterized in *Xenopus* and fission yeast (17, 18). Several subsequent experiments have shown that Cdt1 interacts with

The atomic coordinates and structure factors (code 2RQQ) have been deposited in the Protein Data Bank, Research Collaboratory for Structural Bioinformatics, Rutgers University, New Brunswick, NJ (http://www.rcsb.org/).

[1] Both authors contributed equally to this work.

[2] To whom correspondence may be addressed. Tel.: 81-42-677-4873; Fax: 81-42-677-4873; E-mail: jee-jungoo@tmu.ac.jp.

[3] Present address: Cellular Dynamics Laboratory, RIKEN.

[4] Present address: Chromosome Dynamics Laboratory, RIKEN.

[5] To whom correspondence may be addressed. Tel.: 81-3-3986-0221; Fax: 81-3-5992-1029; E-mail: fumio.hanaoka@gakushuin.ac.jp.

[6] The abbreviations used are: ORC, origin recognition complex; Cdc6, cell division cycle 6 homolog; Cdt1, chromatin licensing and DNA replication factor 1; Mcm2, minichromosome maintenance 2; GST, glutathione *S*-transferase; WHD, winged-helix domain; r.m.s.d., root mean square devation.

Mcm2–7 both *in vitro* and *in vivo* (19–22). Cdt1 can be divided into three functional regions, namely, N-terminal, central, and C-terminal regions, which have DNA-, geminin-, and Mcm2–7-binding activity, respectively (20, 22). In addition to its role in binding to DNA, the N-terminal region is employed to interact with proliferating cell nuclear antigen (23) and Cdc7 and contains ubiquitination and acetylation sites. The function of Cdt1 is negatively controlled by a small protein termed geminin (24) and by the ubiquitin-mediated degradation pathway (25). In metazoans, the degree of sequence conservation in the C-terminal fragment of Cdt1 is higher than in the N-terminal and central regions (22). However, even in the C-terminal region, homology decreases abruptly in budding yeast, showing sequence identity of <20% compared with the mouse sequence. In fact, *S. cerevisiae* Cdt1 could not be uncovered using only a simple database search (21). Of the three functional regions in Cdt1, structural information is available for the central region, which was determined by x-ray crystallography as a complex with geminin by Lee *et al.* (26). They also showed the long helical region of geminin is involved in hindering the interaction between Cdt1 and Mcm2–7.

Because of a resemblance in DNA replication initiation between archaea and eukaryotes, the data from archaea, particularly structural information, have assisted our understanding of the events in eukaryotes (27). The structures of ORC (28, 29), Cdc6 (13), and Mcm (14) from archaea are very informative; however, it is impossible to deduce the function of Cdt1 using this strategy because of a lack of orthologues in archaea. So far, the regions of Cdt1 for Mcm2–7 binding have been characterized mainly by using deletion mutants (20, 22). At a residue-specific level, to date, only one study has reported the importance of two conserved lysines (30).

To understand the function of Cdt1 in detail, we carried out a structural and mutagenesis study. In this study, we used multidimensional NMR spectroscopy to determine the structure of the C-terminal fragment (residues 450–557) of mouse Cdt1. We then performed an *in vitro* binding assay with Mcm proteins with mutants prepared based on the NMR structure. Finally, we carried out *in vitro* and *in vivo* assays to demonstrate that the additional residues in the N-terminal direction from the structural region are equally important for the recognition of Mcm proteins.

EXPERIMENTAL PROCEDURES

DNA Cloning and Protein Purification for Structure Determination—DNA corresponding to the C-terminal fragment of mouse Cdt1 (residues 450–557, mCdt1$^{C\text{-}WHD}$) was cloned into a pGEX-6p-1 vector and then transformed into *Escherichia coli* BL21 strain. The fusion proteins were purified by GSH affinity chromatography. The N-terminal GST was removed by cleavage with recombinant rhinovirus 3C protease. Further purification steps using Q-Sepharose and Sephadex 75 column chromatography were applied. Finally, the buffer was replaced with 50 mM phosphate buffer, pH 6.5, for NMR measurement. Site-directed mutagenesis was performed using the QuikChange mutagenesis kit (Stratagene) according to the manufacturer's instructions. All the mutants and the Mcm4/6/7 complex for the *in vitro* binding assay were cloned and purified using methods identical to those described previously (22). We performed densitometric analysis for GST pulldown data by using Multi Gauge (Fujifilm) and quantified binding affinities between Cdt1 mutants and Mcm4/6/7 proteins.

Yeast Strains—Strains were constructed using standard genetic techniques. W303-1A (*MATa ade2-1 ura3-1 his3–11, 15 trp1-1 leu2–3 112can1–100*) and YIp128-based strains (*ade2-1 ura3-1 his3–11, 15 trp1-1 112can1–100, TAH11::GAL-TAH11 HIS3, leu2::LEU2 TAH11-FLAG*) were grown at 30 °C in YP (1% (w/v) yeast extract (Difco); 2% (w/v) Bacto-peptone (Difco)) containing the indicated carbon source at a final concentration of 2% (w/v). cDNA for Tah11 was amplified by PCR and subcloned into pYIp128.

NMR Spectroscopy and Resonance Assignment—NMR spectra were acquired with Bruker DRX 500-, DRX 800-, or Varian 900-MHz spectrometers equipped with pulse-field gradient, triple resonance probes. Assignment of the ^{1}H, ^{15}N, and ^{13}C resonances of mCdt1$^{C\text{-}WHD}$ was made by a series of triple resonance experiments, CBCA(CO)HN, HNCACB, HNCO, C(CCO)NH, H(CCCO)NH, and HCCH-TOCSY (31). The ^{15}N-edited NOESY-HSQC (100- and 150-ms mixing times) and ^{13}C-edited NOESY-HSQC (150-ms mixing time) spectra were used to derive distance restraints for structure determination and assignment. All the data were processed with NMRPipe (32) and analyzed with NMRView (33).

Structure Calculation—Structures were calculated by CYANA 2.0 (34) and further refined by the AMBER 7 package (35). All the NOE cross-peaks were checked manually using NMRView (33) and assigned using the CANDID algorithm (36) of CYANA. Several tens of CANDID runs were carried out according to the criteria reported (37). A total of 1,826 meaningful NOE upper distance restraints was obtained by CANDID (415 intra-residual, 512 sequential, 523 medium range, and 375 long range). Backbone torsion angle restraints of 159 were derived by the TALOS program (38) and used for all the calculations. Finally, 100 structures that did not show significant violations against experiment restraints were generated using 15,000 steps torsion angle dynamics by CYANA and further refined by AMBER with an all-atom force field. To approximate solvent effects, the generalized Born implicit solvent model was used (39). The best 20 structures were selected and analyzed using AQUA and PROCHECK-NMR software (40). The structure closest to the mean coordinate was selected as a representative. The coordinates and NMR restraints for structure calculation were deposited in the PDB data base (ID: 2RQQ). All the figures were created by using PyMOL software (41).

RESULTS

Preparation of Stable Protein Fragment for NMR Study—Initially the region containing residues 407–557 of mCdt1 (mCdt1^{CTF}) was chosen for the NMR study. However, the residues 407–449 (mCdt1$^{C\text{-}N}$) of the region were sensitive to protease and easily degraded at the protein concentration needed to measure three-dimensional NMR experiments in the required time. Therefore, we focused our attention on the region containing residues 450–557 (mCdt1$^{C\text{-}WHD}$) for structure determination, even though the region containing residues 407–557 is needed for binding to Mcm proteins. The construct

TABLE 1
Statistics of mCdt1$^{C\text{-}WHD}$ final 20 structures
All variations are S.D. unless shown otherwise.

NOE restraints	1826
Intra (|i-j| = 0)	416
Sequential (|i-j| = 1)	512
Medium range (2≤|i-j|≤4)	523
Long range (|i-j|≥5)	375
Dihedral angle restraints	79/80 (ϕ/φ)
AMBER energies (kcal/mol)[a]	
Total energy	−4712 ± 19
Constraint energy	24 ± 2
Numbers of violations	
Distance violation (>0.5 Å)	0
Angle violation (>5.0°)	0
Maximum violations	
Distance violation (Å)	0.406
Angle violation (°)	4.842
Coordinate precision[b]	
Backbone atoms (Å)	0.35
Heavy atoms (Å)	0.87
Ramachandran plot (%)	
Most favored	92.7
Additionally favored	6.5
Generously favored	0.4
Disallowed	0.4

[a] Represents the generalized Born model energy of AMBER 7.
[b] Residues 454–555 are considered.

of residues 407–557 was used instead for the *in vitro* binding assay. The sample of mCdt1$^{C\text{-}WHD}$ was stable for several weeks at high concentration. The results of size-exclusion chromatography indicated that mCdt1$^{C\text{-}WHD}$ exists as a monomer (data not shown).

Winged-helix Domain in C-terminal Fragment of Cdt1—Final structures are well refined, with a backbone and heavy atom root mean square deviation (r.m.s.d.) in residues Pro-454 to Glu-555 of 0.35 Å and 0.87 Å, respectively. The structures also have good geometry with 92.6% of residues in the most favored region of the Ramachandran plot (Table 1 and Fig. 1*A*). N-terminal residues to Cys-453 and C-terminal residues of Gly-556 and Leu-557 are not well converged in the ensemble due to absence of long range NOE. The secondary structures comprise four α-helices (H1, residues 455–480; H2, 487–496; H3, 504–517; and H4, 541–552) and three β-strands (S1, 485–486; S2, 522–526; and S3, 531–535). Pro-467 is positioned in the middle of H1, causing a slight kink of H1 around the residue. The topology of the secondary structures, including the wing region between S2 and S3 (W1, 527–530) is H1-S1-H2-H3-S2-W1-S3-H4 and constitutes a typical winged-helix domain (hereafter WHD) (Fig. 1*B*). Residues located at the interior layer of each helix contribute to stabilization of the helices by forming hydrophobic interactions (Fig. 1*C*). Between helices H1 and H4, pairs of residues, Leu-463 and Val-552, and Leu-466 and Leu-548, are in contact with each other, respectively. For helices H1, H3, and H4, three residues, Leu-513, Leu-514, and Leu-517, of H3 interact with Leu-466 of H1 and Leu-548 of H4, respectively. Between H1 and H2, residues Leu-469 and Met-494 also form hydrophobic interactions. The Trp-521 on the loop connecting H3 and S2 stabilizes the secondary structures by contact with Ala-470 and Leu-473 of H1, and Asp-536, Val-539, and Leu-544 of H4. In addition to the hydrophobic interactions described, a hydrogen bond between Nε1 of Trp-521 and backbone carbonyl of Asp-536 participates in tightening of the secondary structures. The presence of this bond is supported by its observation in all the final 20 NMR structures. Intriguingly, the mCdt1$^{C\text{-}WHD}$ sequence contains 19 leucines, with many of these residues being involved in hydrophobic interactions between secondary structures. Surface electrostatic charges reveal that, on the outward face from the end of helix H1 and the next loop connecting helices H1 and H2 and the loop between S3 and H3, there is a positively charged patch consisting of Arg-471, Arg-474, Arg-481, and Lys-537 of mCdt1$^{C\text{-}WHD}$. With the exception of this region, there is no noticeable charged patch (Fig. 1*D*).

Sequence Alignment and Conservation of Cdt1$^{C\text{-}WHD}$—To know sequence conservation from the viewpoint of function and evolution, the regions corresponding to mCdt1$^{C\text{-}WHD}$ (residues 450–557) were extracted from six representative species and aligned using MUSCLE software (42). The alignment was adjusted manually on the basis of structural information. The extracted sequences are as follows. Mouse, Met^{450}–Leu^{557}; Human, Met^{438}–Leu^{546}; *Xenopus*, Met^{512}–Ser^{619}; *Drosophila*, Met^{636}–Asn^{743}; *Caenorhabditis elegans*, Ala^{546}–Ser^{665}; *S. pombe*, Lys^{324}–Ser^{437}; and *S. cerevisiae*, Ser^{499}–Asp^{604} (Fig. 1*E*). The sequence identities against mCdt1$^{C\text{-}WHD}$ are 83% for human Cdt1$^{C\text{-}WHD}$, 59% for *Xenopus*, 44% for *Drosophila*, 24% for *C. elegans*, 20% for *S. pombe*, and 19% *for S. cerevisiae*. Two regions between S3 and H4 in *C. elegans* are not well aligned, and two yeast sequences show lower similarity than those from metazoan. In particular, the H1 region of *S. cerevisiae* is not well aligned with the others. Nonetheless, those residues that have important roles in forming the tertiary structure are well converged in ensemble conformers of mCdt1$^{C\text{-}WHD}$ and are also conserved in sequence alignment. This suggests all the Cdt1$^{C\text{-}WHD}$s have similar structures.

Structures Sharing Similarities with Cdt1$^{C\text{-}WHD}$—The DALI server (43) was used to search for the protein structures similar to that of mCdt1$^{C\text{-}WHD}$. This search retrieved 562 WHD structures with Z-scores higher than 2.0 from the PDB data base in March of 2009 (44). Strikingly, the closest similarity was found in the structure of the C-terminal domain of the archael Cdc6 orthologue (PDB: 1FNN, Z score: 6.8, r.m.s.d.: 3.0 Å (over 81 residues)). WHDs in proteins, zinc uptake regulation protein Furb (2O03, Z score: 6.6, r.m.s.d.: 2.7 (76 residues)), *Staphylococcus* Sars protein (1P4X, Z score: 6.6, r.m.s.d.: 4.2 (76 residues)), and viral protein F93 (2CO5, Z-score: 6.5, r.m.s.d.: 2.8 (76 residues)), were followed. Despite not being included in the structures of closest similarity, it should be noted that the central region of mouse Cdt1 (residues 179–365, mCdt1$^{M\text{-}WHD}$) from the complex structure with geminin (PDB: 1WLQ) were also retrieved from the DALI server and had a Z-score of 4.9 and r.m.s.d. of 3.4 Å in 93 residues. To obtain detailed information from similar structures, we extracted 21 sequences in the structures with Z-scores higher than 6.0. Of these, considering sequence redundancies, we selected 16 and aligned the sequences based on the structural overlays. For comparison, we included the sequence from mCdt1$^{M\text{-}WHD}$. In each sequence any amino acid that had a corresponding mCdt1$^{C\text{-}WHD}$ amino acid was extracted (Fig. 2*A*). The alignment revealed that residues in the loop regions of mCdt1$^{C\text{-}WHD}$ were less aligned, suggesting that the loop conformations in mCdt1$^{C\text{-}WHD}$ and other

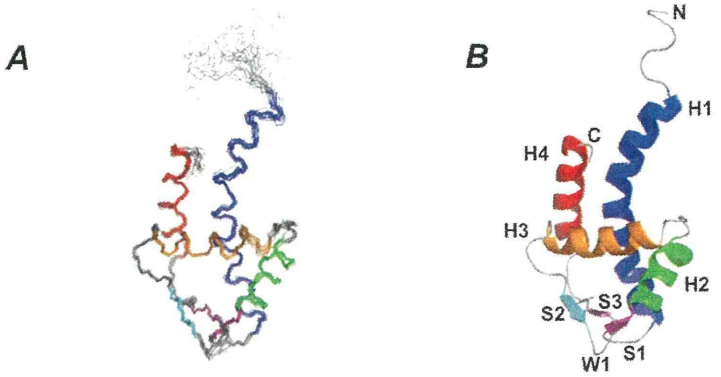

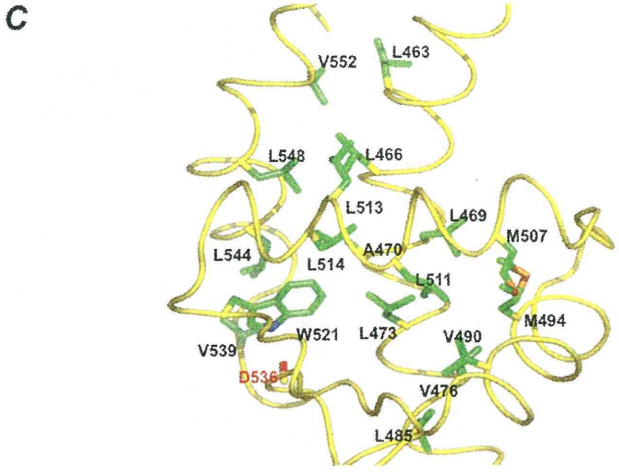

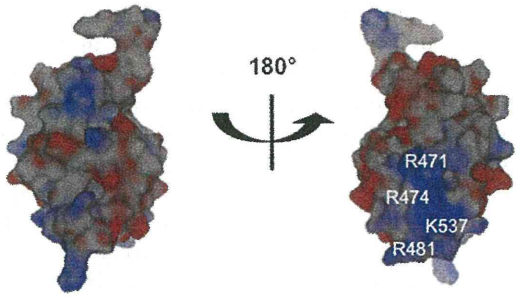

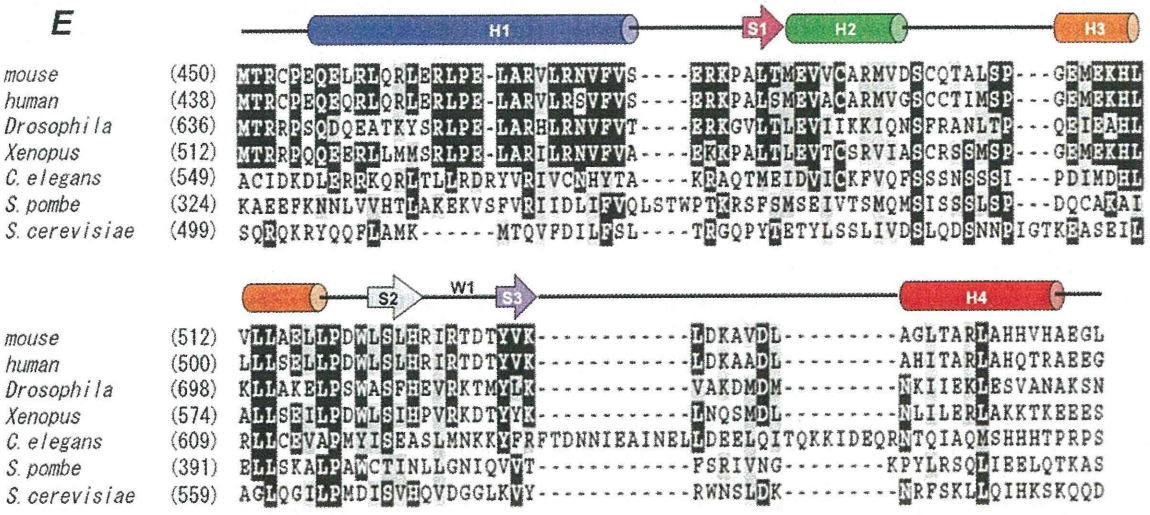

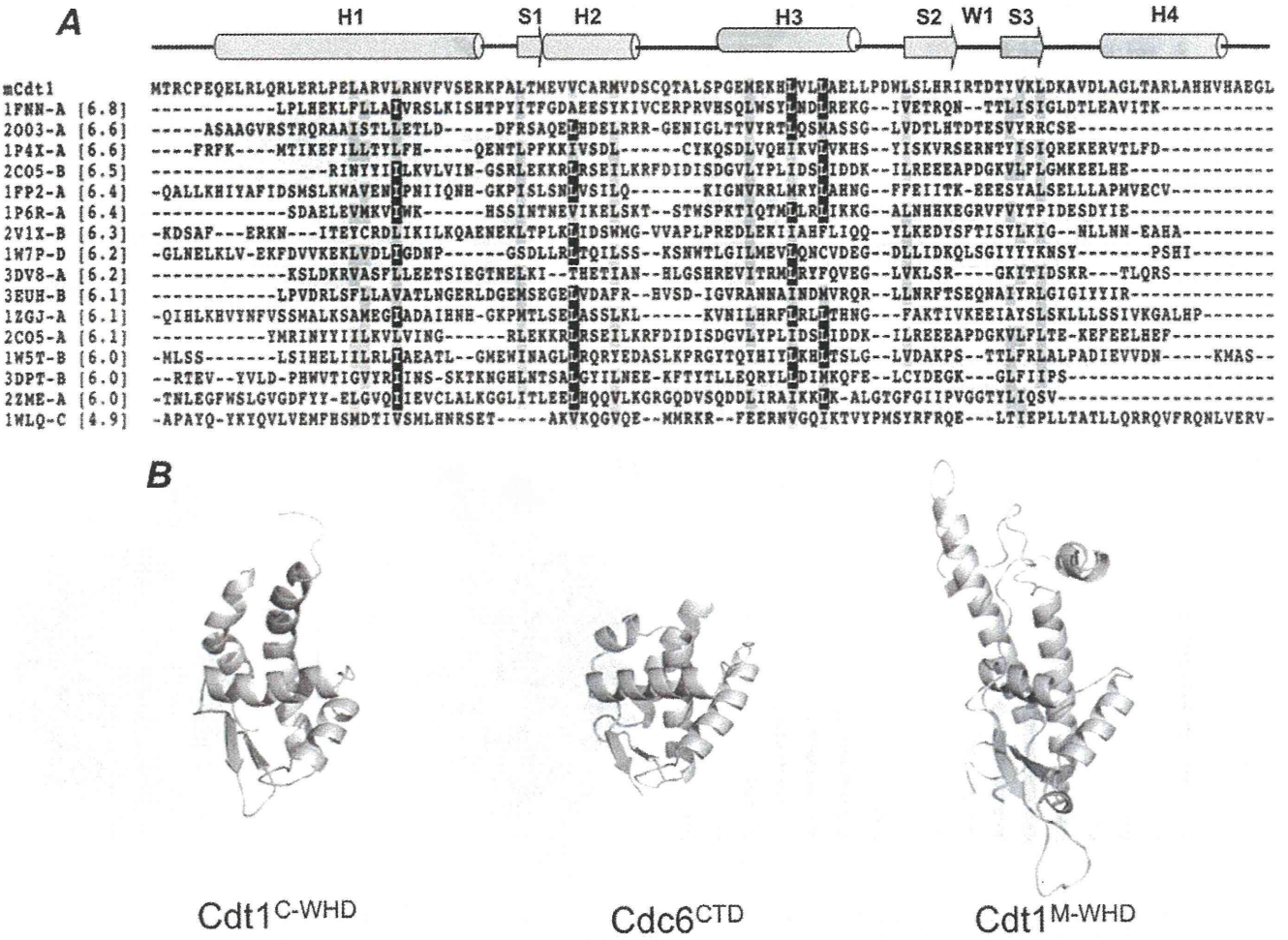

FIGURE 2. **Comparison of sequences and structures between Cdt1$^{C\text{-}WHD}$ and other winged-helix domains.** *A*, the sequences from DALI (43)-driven homologous structures ($Z \geq 6.0$) are aligned when there is a corresponding sequence in mCdt1$^{C\text{-}WHD}$. For comparison, the sequence from the central fragment from mouse Cdt1 (1WLQ) is included. PDB codes and the chain names of WHD are shown. The values in *parentheses* represent the Z-scores. When the portion of an amino acid is >50%, the amino acid is colored *black*. The residues with similar properties are shown in *gray*. *B*, winged-helix domains found in DNA replication licensing. mCdt1$^{C\text{-}WHD}$ in the current study (*left*), C-terminal WHD of Cdc6 (Cdc6^{CTD}, PDB: 1FNN) (*center*) and mCdt1$^{M\text{-}WHD}$ (PDB: 1WLQ) (*right*) are drawn using a *ribbon diagram*. Coordinates are aligned to have the same direction with mCdt1$^{C\text{-}WHD}$.

WHDs are diverse. Of the secondary structures, the helix H4 is hardly aligned even in the C-terminal domain structure of Cdc6 (1FNN) (Fig. 2). It is clear that the properties of hydrophobic residues involved in maintaining the tertiary fold in mCdt1$^{C\text{-}WHD}$ are still conserved in the other WHDs despite overall lower sequence similarities, implying that their roles are to maintain tertiary folds. In the next section, we discuss WHDs in detail. mCdt1$^{M\text{-}WHD}$ (1WLQ) has additional residues in N and C termini and longer inserted loop between S2 and S3 (Fig. 2). However, secondary structures in winged-helix regions are similar to each other and other WHDs in length and positions (Fig. 2). Structure-based sequence alignment reveals 16% sequence identity between the two domains mCdt1$^{M\text{-}WHD}$ and mCdt1$^{C\text{-}WHD}$, whereas sequence-only alignment could not align correctly even the secondary structural regions. Under "Discussion," we provide a detailed review of these findings from an evolutionary viewpoint.

In Vitro Binding Assays with C-terminal Regions of Cdt1 and Mcm4/6/7—In a previous experiment, we showed that the C-terminal fragment of Cdt1 binds to Mcm proteins (22). In the present study, we characterized the region in greater detail (Fig. 3, *A–C*). Because reconstituting Mcm2–7 *in vitro* is not possi-

FIGURE 1. **NMR structures of mCdt1$^{C\text{-}WHD}$.** *A*, superimposed final 20 structures. The structures are overlaid by backbone atoms of residues Pro^{454} to Glu^{555}. Four helices are drawn with different colors, H1 (residues 455–480) in *blue*, H2 (487–496) in *green*, H3 (504–517) in *brown*, and H4 (541–552) in *red*. In three β-strands, S1 (485–486) is drawn in *pink*, S2 (522–526) in *purple*, and S3 (531–535) in *cyan*. The wing region between S2 and S3 is labeled as *W1*. *B*, a *ribbon diagram* of the representative NMR structure. The secondary structures are colored using the same code as in *A*. *C*, residues involved in stabilizing inter secondary structures are drawn as *stick models*. Asp-536 whose backbone carbonyl forms hydrogen bonds with Nϵ1 of Trp^{521} is labeled in *red*, and the others are in *black*. *D*, electrostatic surface calculated from APBS (56) is drawn in the range of $-4k_B/T$ (*red*) to $4k_B/T$ (*blue*). All the figures of the structure were created by using PyMOL (41). All the coordinates were aligned to have the same direction. *E*, sequence alignment of Cdt1$^{C\text{-}WHD}$. Residues that correspond to 450–557 of mouse Cdt1 were extracted in human, *Xenopus*, *Drosophila*, *C. elegans*, *S. pombe*, and *S. cerevisiae* and aligned using MUSCLE (42). The number of starting residues in each sequence line is written in *parentheses*. Secondary structures are *drawn* on the sequences. Residues showing identities of >70% are colored *black*, and those >50% are *gray*.

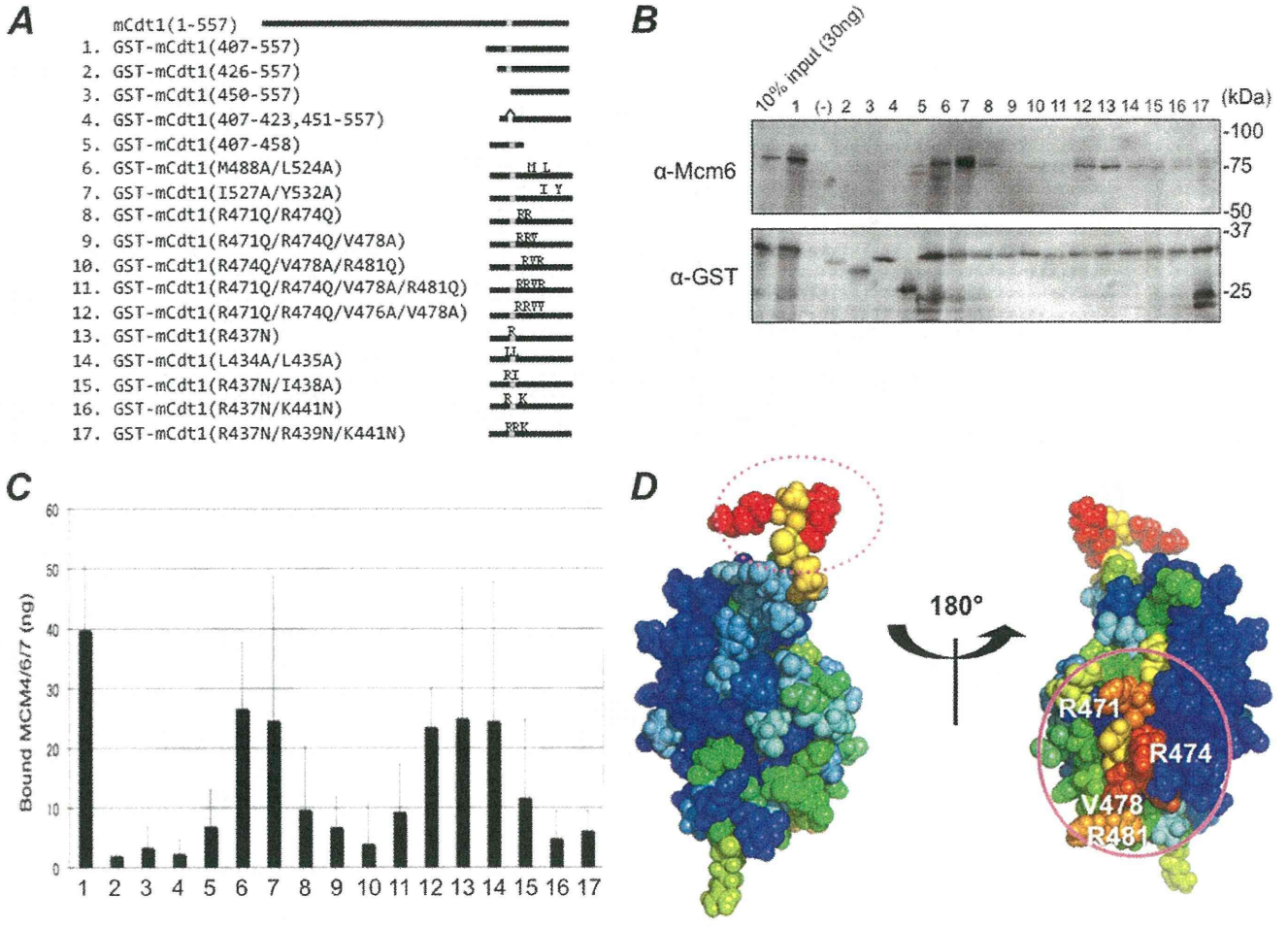

FIGURE 3. **In vitro binding assay with the fragments and the structure-based point mutants of mCdt1^{CTF} and Mcm4/6/7.** *A*, peptide constructs used in this experiment. *B*, pulldown analysis. GST-tagged mCdt1^{CTF} peptides were mixed with purified Mcm4/6/7 complex and incubated with glutathione-Sepharose to precipitate complexes containing mCdt1 peptides. The complexes were washed and visualized by Western blotting using anti-Mcm6 (*α-Mcm6*) and anti-GST (*α-GST*) antibodies. The reaction was done under in 200 mM NaCl, 20 mM Tris HCl, pH 7.5, 0.1% Nonidet P-40, 0.25% gelatin. The constructs having point mutations were generated with GST-mCdt1 (407–557). *C*, the amounts of bound Mcm4/6/7 and errors were quantified by repeating the reaction under identical conditions. *D*, surface-exposed and conserved residues that form a patch are shown. The *colors* in the order of *blue* to *red* indicate the lower to higher degrees of conservation. The first putative protein-protein interaction site is marked by a *dashed circle*, and the second site is marked by a *continuous circle*.

ble, we selected the Mcm4/6/7 complex based on reports that reconstituted Mcm4/6/7 has DNA helicase activity (11, 12, 30). Initially, the region of mCdt1 that acted as a Mcm4/6/7 binding site was narrowed to a fragment of residues 407–557. This region showed comparable binding affinity toward Mcm4/6/7 to that of wild type. However, the fragment, whose structure was determined in this study (mCdt1$^{C\text{-}WHD}$, residues 450–557), hardly bound to Mcm4/6/7 (Fig. 3, *B* and *C*, *lane* and *bar 3*). We selected only the protease-sensitive extra region of 407–458, but it also did not show binding affinity (Fig. 3, *B* and *C*, *lane* and *bar 5*). We further prepared two additional constructs, the former or the latter half of mCdt1$^{C\text{-}N}$ and the region of mCdt1$^{C\text{-}WHD}$ (407–423/451–557 and 426–450/451–557), and investigated their activities. Both constructs bound little with Mcm4/6/7 (Fig. 3, *B* and *C*, *lanes* and *bars 2* and *5*). Altogether, the existence of both residues 407–449 and 450–557 are indispensable for binding to Mcm4/6/7. The PSIPRED software (45) predicted the secondary structure of residues 424–448 as a helix, whereas the first part (407–423) that includes many prolines is likely to form neither helix nor strand. Judging from the sensitivity to protease, the region of mCdt1$^{C\text{-}N}$ probably does not make stable interaction with the rest of the region in the construct 450–557. Ferenbach *et al.* reported that the region required for *Xenopus* Cdt1 to bind to Mcm2/4/6/7 consists of residues 447–620 (20). However, residues 407–557 that we identified in mouse Cdt1 correspond to residues 469–619 in *Xenopus*, suggesting that the residues 447–468 of *Xenopus* Cdt1 are not necessary for binding to Mcm2/4/6/7.

Regions of Winged-helix Domain for Binding to Mcm Proteins—Both BLAST and PSI-BLAST searches when queried with residues 450–557 of mouse Cdt1 could not retrieve meaningful homologous sequences other than those derived from Cdt1 of various species. Currently available bioinformatics tools do not list noticeable consensus motifs from the sequence (data not shown). As a result, knowing only the sequence is not informative for speculating the functional residues of Cdt1$^{C\text{-}WHD}$. Therefore, we combined structural information with sequence data. This procedure is based on the idea that the residues important for scaffold or function in protein are restrained during evolution. Therefore, searching for residues that are identi-

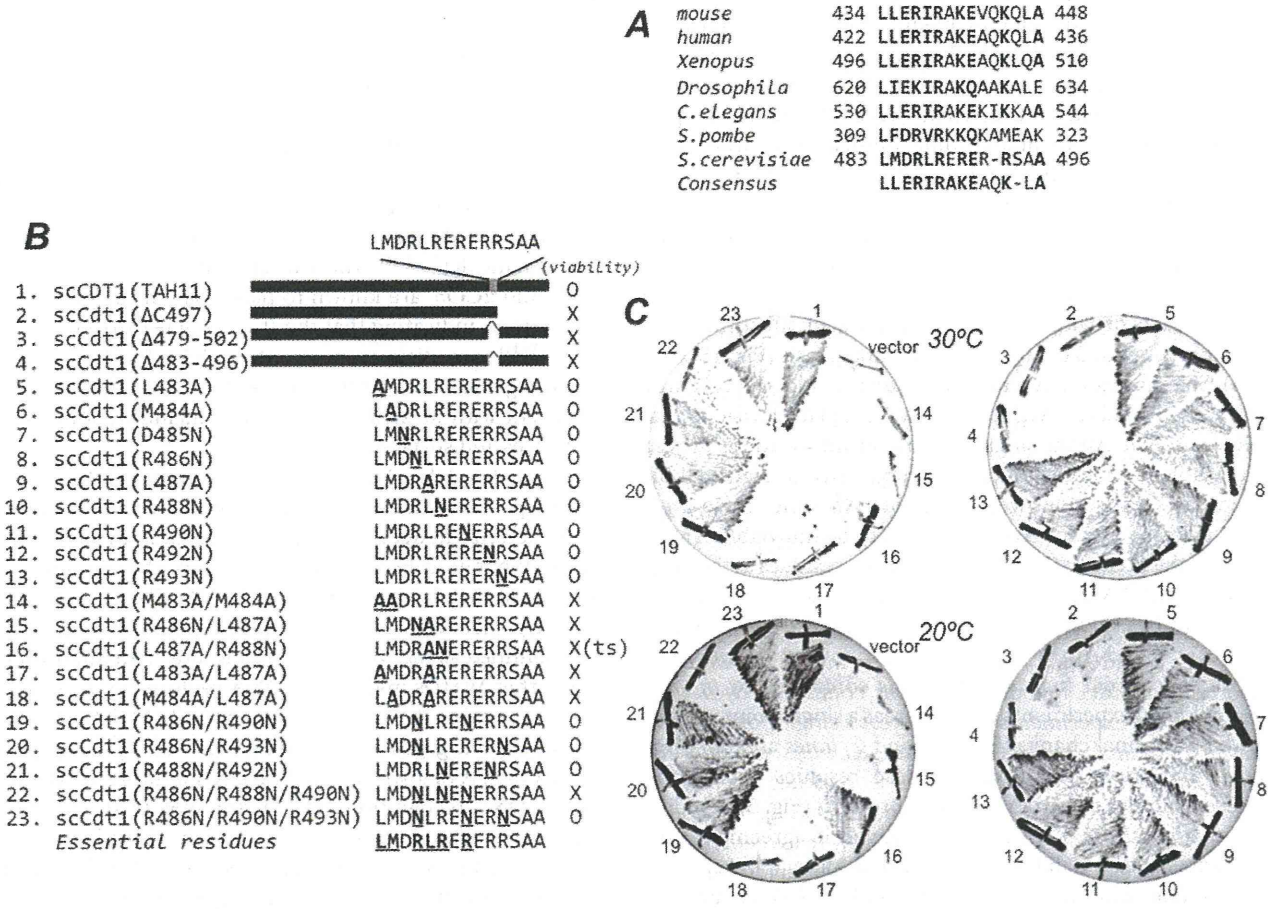

FIGURE 4. **Yeast viability assay.** *A*, the alignment of sequences corresponds to residues 434–448 in mCdt1. The consensus sequence is shown in the *bottom line*. *B*, summary of yeast viability assay. *Lines 1–4* contain vectors for deletion mutations. *5–23* are prepared for point mutations at the residues that are *underlined* with *bold characters*. *C*, yeast expression in glucose media lacking Leu. The same residue numbers are used in *B* and *C*. The yeast harboring vector 16 was viable at 30 °C, but nonviable at 20 °C, indicating temperature sensitivity (*ts*).

cal or have conserved properties on the exposed surface is a reasonable approach for deducing the functional portions from a clueless sequence. For this purpose, we used the WHISCY server (46). It selects only patches formed on conserved and solvent-accessible residues. In addition to the sequences used for alignment (Fig. 1*E*) and the current structure, we added nine more sequences from metazoans to increase precision. Two patches were scored as potential protein-protein interfaces (Fig. 3*D*). The first (*dashed circle*) was the N-terminal three residues of Met^{450}, Thr^{451}, and Arg^{452}, and the other (*continuous circle*) was the region containing the end of helix H1 and its consecutive loop, which include Arg^{471}, Arg^{474}, Val^{478}, and Arg^{481}. Considering protease sensitivity around the region of residues 450–452, the N-terminal three residues will be probably flexible even in the intact condition. The latter region has both hydrophilic and hydrophobic characteristics, overlapped partially with the positively charged surface of $Cdt1^{C\text{-}WHD}$, and is more conserved (Fig. 1). To identify the functional residues for Mcm2–7 proteins, we carried out an *in vitro* binding assay with Mcm4/6/7 proteins with a series of mutants, each of which has two to four amino acid substitutions in the region of $Cdt1^{C\text{-}WHD}$. Indeed, triple and quadruple mutants, R471Q/R474Q/V478A, R474Q/V478A/R481Q, and R471Q/R474Q/V478A/R481Q, showed markedly reduced binding activities to Mcm4/6/7 (Fig. 3, *B* and *C*, *lanes* and *bars 9–11*). Considering that R471Q/R474Q influenced a little (Fig. 3*B*, *lane 8*), Val^{478} will probably play the central role in interacting with Mcm proteins, further supplemented by electrostatic contacts with basic residues. In contrast, other mutants containing mutations in residues Met^{488}, Leu^{524}, Ile^{527}, and Tyr^{532}, chosen simply from sequence conservation, resulted in marginal changes in binding affinity compared with that observed in the wild type (Fig. 3, *B* and *C*, *lanes* and *bars 6* and *7*).

Yeast Viability Assay with Mutants at Additional Fragment—To better characterize the flanking region, $Cdt1^{C\text{-}N}$ (residues 407–449 in mCdt1), especially the highly conserved second half part, Leu^{434} to Ala^{448}, we performed a yeast viability assay. The alignment of eukaryotic sequences, including yeast sequences, reveals high sequence conservation of the region (Fig. 4*A*), which is distinct from $Cdt1^{C\text{-}WHD}$ where sequence similarity is low between mammals and yeast (Fig. 1*E*). Hydrophobic residues (Leu, Met, and Ile) and basic residues (Arg) are particularly conserved. We undertook a systematic mutagenesis of the region for Cdt1, Tah11 (hereafter *scCDT1*), in *S. cerevisiae* and then observed cell viability. Note that *scCDT1* is an essential gene. The promoter of endogenous *scCDT1* gene in W303a was replaced with the GAL1 promoter. Integration of the mutant *scCDT1* gene with the wild-type *scCDT1* promoter and cyc1

terminator at the LEU2 locus allowed the strain to produce mutant proteins in the glucose medium. At first, a C-terminal truncated mutant (Fig. 4*B*, *row 2*) or mutants that lack the conserved region (Fig. 4*B*, *rows 3* and *4*) were checked for growth defects. Both deletion constructs were unable to support growth in glucose medium, while full-length *scCDT1* (Fig. 4*B*-1) could be substituted for endogenous protein. These results indicate again that both regions of scCDT1, which correspond to $Cdt1^{C\text{-}WHD}$ and highly conserved $Cdt1^{C\text{-}N}$, are essential for scCDT1 function. To examine the functional effects of substitutions in the conserved region, 19 alleles of *scCDT1*, each of which contains amino acid substitution(s), were then generated by site-directed mutagenesis (Fig. 4*B*, *rows 5–23*). We substituted Ala for conserved Leu and Met residues, and charged residues, Arg and Asp, were replaced with neutral amino acid Asn. All the single amino acid substitutions proved to be viable. In contrast and intriguingly, five of eight double amino acid substitutions were nonviable. Also one of two triple amino acid changes for Arg was shown to be nonviable. Taken together, the existences of the hydrophobic residues at the positions of Leu^{483}/Met^{484}/Leu^{487} in scCdt1 and Leu^{434}/Leu^{435}/Ile^{438} in mCdt1, and the basic residues at Arg^{486}/Arg^{488}/Arg^{490} in $scCdt1^{CTF}$ and Arg^{437}/Arg^{439}/Lys^{441} in $mCdt1^{CTF}$ would be important for Cdt1 function. This was confirmed by *in vitro* GST pulldown experiments too. Whereas a single point mutant showed a nominal change (Fig. 3, *B* and *C*, *lanes* and *bars 13*), double and triple mutations in these residues caused the reduced affinities toward Mcm4/6/7 proteins (Fig. 3, *B* and *C*, *lanes* and *bars 15–17*), which is qualitatively in agreement with the results of yeast viability assay. You and Masai (30) reported that a double point mutant of mCdt1, K441A/K445A, failed to generate a complex with Mcm proteins. Lys^{441} is one of those residues that we identified as an important residue in this study. Interestingly, the combined feature of hydrophobic and basic residues (Leu^{434}, Leu^{435}, Arg^{437}, Ile^{438}, Arg^{439}, and Lys^{441}) is reminiscent of the residues pinpointed in $mCdt1^{C\text{-}WHD}$ (Arg^{471}, Arg^{474}, Phe^{477}, Val^{478}, and Arg^{481}) for binding to Mcm proteins, likely suggesting similar contacting mode. On the other hand, the underlying role of the proline-rich region, residues 407–423, remains a subject for future studies.

DISCUSSION

WHD is a typical DNA recognition motif (47). When WHD binds to double strand DNA, the interactions occur at H3, S2, S3, and W1 in the majority of cases. H3 is the primary contact site and W1 acts as an additional and supportive site. To the best of our knowledge, a reversal in these roles of H3 and W1 has been reported once in an exceptional case (47). In addition to H3 and W1, the existence of positively charged residues at H3, S2, S3, and W1 are indispensable for DNA recognition. $Cdt1^{CTF}$ binds to neither double nor single strand DNA (22). To determine the differences between $mCdt1^{C\text{-}WHD}$ and other WHDs, we superimposed the coordinate of $mCdt1^{C\text{-}WHD}$ into each WHD position of known DNA-protein complex structures and investigated the hypothetical contact sites between $mCdt1^{C\text{-}WHD}$ and DNA. In contrast to WHDs that bind to DNA, the lengths of H1 or H4 of $mCdt1^{C\text{-}WHD}$ are considerably longer, with these helices being more inclined to the direction of the plane that consisted of H3 and S2, S3, and W1. Because of these features, one or both of H1 and H4 of $mCdt1^{C\text{-}WHD}$ would encounter steric clashes with DNA, if it binds to DNA in the same manner as the other WHDs do. In fact, as shown in the structure-based sequence alignment (Fig. 2*A*), the residues in H1 and H4 are not fully aligned, meaning that they are unique to $mCdt1^{C\text{-}WHD}$. Furthermore, there is no particularly charged patch on the surface regions of H3, S2, S3, and W1 (Fig. 1*C*). It should be noted that the WHDs that share the closest similarities with $mCdt1^{C\text{-}WHD}$, those from PDB codes of 1FNN, 2O03, 1P4X, and 2CO5, are known to participate in protein-protein interactions, indicating that the structural features of WHD in $Cdt1^{C\text{-}WHD}$ are distinct from other DNA binding domains. Taken together, the inability of $Cdt1^{C\text{-}WHD}$ in DNA binding is consistent with its structural features, including long H1 and H4 helices and surface charge.

Accumulated data have revealed that some WHDs serve as a protein-protein interaction module. We need more examples to characterize in detail the region involved in protein-protein interaction, but at least in two such cases, the apoptotic protease-activating factor 1 (48) and ESCRT-II–III system (49), protein-protein interactions occur at similar areas of WHD to that identified as the Mcm2–7 binding site. The question then is, do other WHDs involved in DNA replication licensing use the same region to interact with Mcm2–7? The WHD of archael Cdc6 engages in interaction with Mcm proteins as well as DNA (50). As shown with typical DNA binding WHDs, H3 is a major DNA recognition site in Cdc6 WHD (51, 52), but the region that interacts with Mcm proteins has not been characterized. The structural resemblance between WHDs of archael Cdc6 and $mCdt1^{C\text{-}WHD}$ and the high degree of sequence homology between archael and eukaryotic Cdc6s (13) tempt us to presume that similar regions in WHDs are employed for Mcm proteins. In yeast, the Cdc6 WHD can interact with both DNA and Mcm2–7 simultaneously (53). When considering the steric effects and the large molecular sizes in DNA replication licensing protein, the prime candidate site of Cdc6 WHD for binding to Mcm2–7 will be placed at the opposite side from the H3 DNA binding site and likely include the region identified as the Mcm binding site in $Cdt1^{C\text{-}WHD}$. Yet there has been no report that $Cdt1^{Central}$ has a helicase-binding activity. Nevertheless, both $Cdt1^{Central}$ and $Cdt1^{CTF}$ are required to load Mcm2–7 for licensing activity (20). Moreover, Lee *et al.* reported that the interaction between Cdt1 and Mcm2–7 is inhibited by steric hindrance caused by a contact between geminin that binds to the central region of Cdt1 and Mcm proteins (26). This raises the possibility that two fragments of $Cdt1^{Central}$ and $Cdt1^{CTF}$ are located in close proximity, at least when Cdt1 interacts with Mcm2–7, implying potential cooperation between the two regions.

Similarities in folding, sequence, and interacting site with partner protein led us to postulate that the central and C-terminal regions of Cdt1 were duplicated in tandem from a domain and have evolved together. This type of duplication occurs frequently in eukaryotic proteins and confers functional diversities (54). In addition to the region of WHD in the crystal structure (residues 179–365 of mouse Cdt1), $Cdt1^{Central}$ needs its flanking sequence to bind to geminin *in vivo* (20). Interest-

ingly, this sequence is located in the N-terminal direction from the structural region of $Cdt1^{M\text{-}WHD}$ and corresponds to residues 193–243 in *Xenopus* and 121–181 in mouse Cdt1, respectively. These positions are reminiscent of the relative positions between the protease-sensitive fragment, residues 407–448, and the structural part, residues 450–557, of $Cdt1^{C\text{-}WHD}$ in the current study. However, the central regions of Cdt1 are under weaker evolutionary pressure, because $Cdt1^{Central}$ has lower sequence homology across species than those found in $Cdt1^{CTF}$ (22). Evolutionary trends in Cdt1 fragments are also reflected by the presence or diverseness of their binding partners. Geminin, the partner of $Cdt1^{Central}$, is missing or elusive in budding yeast, whereas the presence of Mcm2–7 with which $Cdt1^{CTF}$ mainly interacts is highly conserved in eukaryotes, consistent with evolutionary conservation in the fragments. In addition to the clues and questions required to understand the interaction between Cdt1 and Mcm2–7 raised by our data, it would be worthwhile studying the roles of WHDs in $Cdt1^{CTF}$, $Cdt1^{Central}$, and Cdc6 as a common evolutionary module.

In summary, we have shown that the C-terminal fragment of Cdt1 forms a WHD, but its structural features are different from other typical DNA binding WHDs. Although the structural region determined in the current study is insufficient to bind to Mcm proteins alone, we were able to characterize the residues of the WHD that are involved in interactions with replicative helicase. We also showed an additional region in the N-terminal direction of the WHD is equally important. How these two parts work cooperatively remains unanswered, and further experiments are required to elucidate this mechanism. Eukaryotic DNA replication initiation machinery is large and complicated, and presently, it is not possible to reconstitute the system *in vitro*. Therefore, dissecting each component and examining the parts is a reasonable strategy. We believe that our data will be a valuable addition to understanding the process and evolution of DNA replication licensing in eukaryotes.

Acknowledgments—We thank Drs. Toshihiko Eki for constructing yeast strains and Naoko Imamoto for encouragement and support.

Addendum—While we were in preparation of the manuscript, a report describing the solution and crystal structures of C-terminal regions of mouse Cdt1 was published (55).

REFERENCES

1. Bell, S. P. (2002) *Genes Dev.* **16,** 659–672
2. Bell, S. P., and Dutta, A. (2002) *Annu. Rev. Biochem.* **71,** 333–374
3. Blow, J. J., and Dutta, A. (2005) *Nat. Rev. Mol. Cell Biol.* **6,** 476–486
4. Nishitani, H., and Lygerou, Z. (2004) *Front. Biosci.* **9,** 2115–2132
5. Takeda, D. Y., and Dutta, A. (2005) *Oncogene* **24,** 2827–2843
6. Blow, J. J., and Gillespie, P. J. (2008) *Nat. Rev. Cancer* **8,** 799–806
7. Ramachandran, N., Hainsworth, E., Bhullar, B., Eisenstein, S., Rosen, B., Lau, A. Y., Walter, J. C., and LaBaer, J. (2004) *Science* **305,** 86–90
8. Bell, S. P., and Stillman, B. (1992) *Nature* **357,** 128–134
9. Cvetic, C., and Walter, J. C. (2005) *Semin. Cell Dev. Biol.* **16,** 343–353
10. Tye, B. K., and Sawyer, S. (2000) *J. Biol. Chem.* **275,** 34833–34836
11. You, Z., Komamura, Y., and Ishimi, Y. (1999) *Mol. Cell. Biol.* **19,** 8003–8015
12. You, Z., and Masai, H. (2005) *Nucleic Acids Res.* **33,** 3033–3047
13. Liu, J., Smith, C. L., DeRyckere, D., DeAngelis, K., Martin, G. S., and Berger, J. M. (2000) *Mol. Cell* **6,** 637–648
14. Fletcher, R. J., Bishop, B. E., Leon, R. P., Sclafani, R. A., Ogata, C. M., and Chen, X. S. (2003) *Nat. Struct. Biol.* **10,** 160–167
15. Pape, T., Meka, H., Chen, S., Vicentini, G., van Heel, M., and Onesti, S. (2003) *EMBO Rep.* **4,** 1079–1083
16. Hofmann, J. F., and Beach, D. (1994) *EMBO J.* **13,** 425–434
17. Maiorano, D., Moreau, J., and Méchali, M. (2000) *Nature* **404,** 622–625
18. Nishitani, H., Lygerou, Z., Nishimoto, T., and Nurse, P. (2000) *Nature* **404,** 625–628
19. Cook, J. G., Chasse, D. A., and Nevins, J. R. (2004) *J. Biol. Chem.* **279,** 9625–9633
20. Ferenbach, A., Li, A., Brito-Martins, M., and Blow, J. J. (2005) *Nucleic Acids Res.* **33,** 316–324
21. Tanaka, S., and Diffley, J. F. (2002) *Nat. Cell Biol.* **4,** 198–207
22. Yanagi, K., Mizuno, T., You, Z., and Hanaoka, F. (2002) *J. Biol. Chem.* **277,** 40871–40880
23. Arias, E. E., and Walter, J. C. (2006) *Nat. Cell Biol.* **8,** 84–90
24. Wohlschlegel, J. A., Dwyer, B. T., Dhar, S. K., Cvetic, C., Walter, J. C., and Dutta, A. (2000) *Science* **290,** 2309–2312
25. O'Connell, B. C., and Harper, J. W. (2007) *Curr. Opin. Cell Biol.* **19,** 206–214
26. Lee, C., Hong, B., Choi, J. M., Kim, Y., Watanabe, S., Ishimi, Y., Enomoto, T., Tada, S., Kim, Y., and Cho, Y. (2004) *Nature* **430,** 913–917
27. Cunningham, E. L., and Berger, J. M. (2005) *Curr. Opin. Struct. Biol.* **15,** 68–76
28. Dueber, E. L., Corn, J. E., Bell, S. D., and Berger, J. M. (2007) *Science* **317,** 1210–1213
29. Gaudier, M., Schuwirth, B. S., Westcott, S. L., and Wigley, D. B. (2007) *Science* **317,** 1213–1216
30. You, Z., and Masai, H. (2008) *J. Biol. Chem.* **283,** 24469–24477
31. Cavanagh, J., Fairbrother, W. J., Skelton, N. J., and Palmer, A. G. (1996) *Protein NMR Spectroscopy*, Academic Press, San Diego, CA
32. Delaglio, F., Grzesiek, S., Vuister, G. W., Zhu, G., Pfeifer, J., and Bax, A. (1995) *J. Biomol. NMR* **6,** 277–293
33. Johnson, B. A. (2004) *Methods Mol. Biol.* **278,** 313–352
34. Güntert, P., Mumenthaler, C., and Wüthrich, K. (1997) *J. Mol. Biol.* **273,** 283–298
35. Pearlman, D. A., Case, D. A., Caldwell, J. W., Ross, W. S., Cheatham, T. E., III, DeBolt, S., Ferguson, D., Seibel, G., and Kollman, P. (1995) *Comp. Phys. Commun.* **91,** 1–41
36. Herrmann, T., Güntert, P., and Wüthrich, K. (2002) *J. Mol. Biol.* **319,** 209–227
37. Jee, J., and Güntert, P. (2003) *J. Struct. Funct. Genomics* **4,** 179–189
38. Cornilescu, G., Delaglio, F., and Bax, A. (1999) *J. Biomol. NMR* **13,** 289–302
39. Bashford, D., and Case, D. A. (2000) *Annu. Rev. Phys. Chem.* **51,** 129–152
40. Laskowski, R. A., Rullmannn, J. A., MacArthur, M. W., Kaptein, R., and Thornton, J. M. (1996) *J. Biomol. NMR* **8,** 477–486
41. DeLano, W. L. (2002) *The PyMOL Molecular Graphics System*, DeLano Scientific LLC, San Carlos, CA
42. Edgar, R. C. (2004) *Nucleic Acids Res.* **32,** 1792–1797
43. Holm, L., and Sander, C. (1993) *J. Mol. Biol.* **233,** 123–138
44. Berman, H. M., Westbrook, J., Feng, Z., Gilliland, G., Bhat, T. N., Weissig, H., Shindyalov, I. N., and Bourne, P. E. (2000) *Nucleic Acids Res.* **28,** 235–242
45. Jones, D. T. (1999) *J. Mol. Biol.* **292,** 195–202
46. de Vries, S. J., van Dijk, A. D., and Bonvin, A. M. (2006) *Proteins* **63,** 479–489
47. Gajiwala, K. S., and Burley, S. K. (2000) *Curr. Opin. Struct. Biol.* **10,** 110–116
48. Riedl, S. J., Li, W., Chao, Y., Schwarzenbacher, R., and Shi, Y. (2005) *Nature* **434,** 926–933
49. Im, Y. J., Wollert, T., Boura, E., and Hurley, J. H. (2009) *Dev. Cell* **17,** 234–243
50. Kasiviswanathan, R., Shin, J. H., and Kelman, Z. (2005) *Nucleic Acids Res.* **33,** 4940–4950
51. Capaldi, S. A., and Berger, J. M. (2004) *Nucleic Acids Res.* **32,** 4821–4832
52. Wilce, J. A., Vivian, J. P., Hastings, A. F., Otting, G., Folmer, R. H.,

Duggin, I. G., Wake, R. G., and Wilce, M. C. (2001) *Nat. Struct. Biol.* **8,** 206–210
53. Randell, J. C., Bowers, J. L., Rodriguez, H. K., and Bell, S. P. (2006) *Mol. Cell* **21,** 29–39
54. Orengo, C. A., and Thornton, J. M. (2005) *Annu. Rev. Biochem.* **74,** 867–900
55. Khayrutdinov, B. I., Bae, W. J., Yun, Y. M., Lee, J. H., Tsuyama, T., Kim, J. J., Hwang, E., Ryu, K. S., Cheong, H. K., Cheong, C., Ko, J. S., Enomoto, T., Karplus, P. A., Güntert, P., Tada, S., Jeon, Y. H., and Cho, Y. (2009) *Protein Sci.* **18,** 2252–2264
56. Baker, N. A., Sept, D., Joseph, S., Holst, M. J., and McCammon, J. A. (2001) *Proc. Natl. Acad. Sci. U.S.A.* **98,** 10037–10041

THE JOURNAL OF BIOLOGICAL CHEMISTRY VOL. 285, NO. 22, pp. 16822–16829, May 28, 2010

A Common Substrate Recognition Mode Conserved between Katanin p60 and VPS4 Governs Microtubule Severing and Membrane Skeleton Reorganization*[S]

Received for publication, January 28, 2010 Published, JBC Papers in Press, March 25, 2010, DOI 10.1074/jbc.M110.108365

Naoko Iwaya[‡§¶], Yohta Kuwahara[§¶‖], Yoshie Fujiwara[§], Natsuko Goda[§‖], Takeshi Tenno[§‖], Kohei Akiyama[¶], Shogo Mase[§‖], Hidehito Tochio[‡], Takahisa Ikegami[‡‡], Masahiro Shirakawa[‡], and Hidekazu Hiroaki[§¶‖**1]**

*From the [‡]Department of Molecular Engineering, Graduate School of Engineering, Kyoto University, Kyoto-Daigaku Katsura, Nishikyo-ku, Kyoto 615-8530, the [§]Department of Biochemistry and Molecular Biology, Graduate School of Medicine, Kobe University, 7-5-1 Kusunokicho, Chuo-ku, Kobe, Hyogo 650-0017, the [¶]Field of Supramolecular Biology, International Graduate School of Arts and Sciences, Yokohama City University, Yokohama, Kanagawa 230-0045, the [‖]Institute for Bioinformatics Research and Development, Japan Science and Technology Corporation, Tokyo 102-0081, the **Global Center of Excellence Program for Integrative Membrane Biology, Kobe University, Kobe, Hyogo 650-0017, and the [‡‡]Institute of Protein Research, Osaka University, Suita, Osaka 565-0871, Japan*

Katanin p60 (kp60), a microtubule-severing enzyme, plays a key role in cytoskeletal reorganization during various cellular events in an ATP-dependent manner. We show that a single domain isolated from the N terminus of mouse katanin p60 (kp60-NTD) binds to tubulin. The solution structure of kp60-NTD was determined by NMR. Although their sequence similarities were as low as 20%, the structure of kp60-NTD revealed a striking similarity to those of the microtubule interacting and trafficking (MIT) domains, which adopt anti-parallel three-stranded helix bundle. In particular, the arrangement of helices 2 and 3 is well conserved between kp60-NTD and the MIT domain from Vps4, which is a homologous protein that promotes disassembly of the endosomal sorting complexes required for transport III membrane skeleton complex. Mutation studies revealed that the positively charged surface formed by helices 2 and 3 binds tubulin. This binding mode resembles the interaction between the MIT domain of Vps4 and Vps2/CHMP1a, a component of endosomal sorting complexes required for transport III. Our results show that both the molecular architecture and the binding modes are conserved between two AAA-ATPases, kp60 and Vps4. A common mechanism is evolutionarily conserved between two distinct cellular events, one that drives microtubule severing and the other involving membrane skeletal reorganization.

Microtubules (MTs)[2] are polymers of α- and β-tubulin heterodimers. MTs exist as networks that dynamically and rapidly reorganize during different phases of the cell cycle. Spontaneous growth as well as shortening at the ends is indispensable for functional rearrangement. For example, they form the mitotic spindle during M phase, which mediates chromosome segregation during cell division based on the nature of dynamic rearrangement of MTs (reviewed in Refs. 1, 2). Many cellular events involving MTs are driven not only by autonomous polymerization and dissociation of tubulin but also by MT-severing enzymes. These enzymes disassemble the MTs to promote large changes in the cytoskeleton in an ATP-dependent manner (3).

There are three known MT-severing enzymes, katanin, spastin, and fidgetin, all of which belong to type I AAA-ATPases (4–7). Katanin was first identified from sea urchin cytosol (8) and consists of two subunits as follows: a 60-kDa catalytic subunit (kp60) containing a single AAA domain, and an 80-kDa regulatory subunit (kp80) (9, 10). Both the subunits are genetically conserved among many higher eukaryotes. Katanin localizes at the centrosomes in an MT-dependent manner (11), which is probably required for recycling and for the poleward flux of tubulin in the spindle by disassembling MTs at their minus ends (12, 13). kp60 homologs are also found in plants, insects, and nematodes but not in yeasts.

kp60 has a common domain organization typical of a type I AAA-ATPase, which consists of an N-terminal substrate binding region followed by a single AAA domain at the C terminus. In general, AAA-ATPases are believed to act as protein unfoldases that promote various cellular events, including dissociation of protein complexes, MT severing, protein degradation, protein translocation across organelle membranes, vesicle fusions, and multivesicular body formation (reviewed in Refs. 14, 15).

Hartman and Vale (13) demonstrated that the N-terminal half of kp60 contains an MT binding region, although the presence of a structural MT binding domain was not proved. The importance of the N-terminal MT binding region of a plant kp60 ortholog has been recently reported (16). In our previous study, we successfully isolated a folded structural domain from the kp60 N-terminal region (termed kp60-NTD) (17). Al-

* A part of this work was performed under the Cooperative Research Program of Institute for Protein Research, Osaka University.
[S] The on-line version of this article (available at http://www.jbc.org) contains supplemental "Experimental Procedures," Figs. 1–8, Table 1, and additional references.
[1] To whom correspondence should be addressed. Tel.: 81-78-382-5813; Fax: 81-78-382-5816; E-mail: hiroakih@med.kobe-u.ac.jp.
[2] The abbreviations used are: MT, microtubule; AAA, ATPase associated with various cellular activities; ESCRT, endosomal sorting complexes required for transport; GST, glutathione *S*-transferase; kp60, katanin p60; MIT domain, microtubule interacting and trafficking domain; r.m.s.d., root mean square deviation; NTD, N-terminal domain; PIPES, 1,4-piperazinediethanesulfonic acid; PDB, Protein Data Bank.

though standard bioinformatics tools (*e.g.* PSI-BLAST (18), Pfam (19, 20), and SMART (21)) failed to detect any similarity between kp60-NTD and other known domains, more sensitive bioinformatics techniques (*e.g.* FORTE (22) and FUGUE (23)) can detect substantial similarities between kp60-NTD and MIT domains. MIT domains are small helical domains involved in protein-protein interactions that are conserved among Vps4, spartin, spastin, and some other proteins (24).

In this study, we present the solution structure of kp60-NTD. We show that this structure is closely related to that of the MIT domain. In this context, the overall molecular architecture of kp60 resembles other MIT domain-containing type I AAA-ATPases, such as the MT-severing enzyme spastin and the ESCRT-III disassembling enzyme Vps4 (Fig. 1*A*). Because the isolated kp60-NTD solely binds tubulin *in vitro*, the domain is a novel tubulin binding domain. Finally, the key residues of kp60-NTD for binding tubulin were determined. A model for MT binding is further discussed, which allows us to propose a model for the mechanism of MT severing by katanin.

EXPERIMENTAL PROCEDURES

Protein Techniques—Expression vectors for the recombinant GST-tagged form of kp60-NTDs of human and mouse were constructed using PRESAT vector methodology (17, 25). The fusion proteins were expressed in *Escherichia coli* BL21 (DE3), followed by affinity purification on glutathione-Sepharose (GE Healthcare), and were dialyzed. These fusion proteins were used for tubulin binding assays. For NMR spectroscopy, 2 liters of culture was incubated with [^{15}N]ammonium chloride and [^{13}C]glucose as the sole nitrogen and carbon sources, respectively, following a standard fermentation protocol at 25 °C. Divalent cation was present as a trace mineral during fermentation. Purification of ^{15}N- and ^{13}C-/^{15}N-labeled kp60-NTDs was achieved by glutathione-Sepharose affinity chromatography followed by thrombin digestion, benzamidine-Sepharose chromatography, cation exchange chromatography using a SP-Sepharose column, and gel filtration using Superdex 75 column (GE Healthcare).

NMR Spectroscopy—Samples for NMR spectroscopy contained either ^{15}N- or ^{13}C-/^{15}N-labeled kp60-NTD at concentrations of 0.5–0.9 mM in 5% D_2O, 95% H_2O, 20 mM sodium phosphate, and 1 mM EDTA with 50 mM NaCl/without NaCl (pH 6.5). Backbone and side chain assignments were obtained from ^{15}N-heteronuclear single quantum coherence spectroscopy, ^{13}C-heteronuclear single quantum coherence spectroscopy, HNCA, HNCO, HNCACB, CBCACONH, HCC(CO)NH, CC(CO)NH, and HCCH-total correlation spectroscopy spectra recorded at 25 °C, using Bruker Avance spectrometers (500 and 800 MHz, Avance; Bruker Biospin, Germany) equipped with cryomagnetic probes (26, 27). Data were processed using NMRPipe (28) and SPARKY (29) software. Interproton distances were obtained from three-dimensional ^{13}C- and ^{15}N-edited nuclear Overhauser effect spectroscopy spectra recorded with a 100-ms mixing time. Structures were calculated using a standard seven iteration cycle protocol of the program CYANA version 2.0.17 (30, 31). All nuclear Overhauser effect cross-peaks were selected manually using SPARKY. In total, 1723 meaningful nuclear Overhauser effect upper distance restraints were obtained, including 304 long range distances. Dihedral angle restraints were calculated on the basis of backbone atom chemical shifts (32) using the TALOS program. The 20 structures with the lowest restraint energies were selected and analyzed using MOLMOL (33) and PROCHECK-NMR software (Table 1) (34). No distance restraint was violated by more than 0.3 Å and no torsional restraint by more than 5.0°. All the figures were prepared using MOLMOL and PyMOL. The atomic coordinates of the 20 best kp60-NTD NMR structures have been deposited in the Protein Data Bank under accession code 2rpa. Chemical shift assignments have been deposited in the BioMagResBank under accession code 11075.

Mutation Studies and Tubulin Binding Assays—Ala-substituted mutants were prepared by PCR amplification of the entire expression plasmid for kp60-NTD (residues 1–72) according to a standard PCR mutagenesis method using QuikChange site-directed mutagenesis kit (Stratagene). Two complementary oligonucleotides with mutated sequences for each mutant were used as primers (supplemental Table 1). The resulting kp60-NTD genes were sequenced to confirm the mutations. All proteins were purified with glutathione-Sepharose (GE Healthcare) and dialyzed against a buffer containing 50 mM Tris-HCl and 150 mM NaCl (pH 7.5). For pulldown assay, 80 pmol of GST (negative control) or GST fusion proteins were mixed with 10 μl of glutathione-Sepharose 4B (GE Healthcare) in 100 μl of binding buffer containing 80 mM PIPES-KOH (pH 6.8), 0.5 mM EGTA, and 2 mM $MgCl_2$ for 1 h at 4 °C. After washing the beads, 182 pmol (10 μg) of porcine tubulin (Cytoskeleton) was mixed in 200 μl of binding buffer for 2 h at 4 °C. The beads were washed three times, and the associated proteins were eluted with 50 mM Tris-HCl and 10 mM reduced glutathione (pH 7.5). The eluted proteins were resolved by SDS-PAGE and stained with silver.

Model Building—A molecular model of the complex of kp60-NTD with a tubulin tetramer was constructed manually using MOLMOL (33) on the basis of the complex between Vps4a-MIT and CHMP1a (PDB code 2jq9). First, the kp60-NTD structure determined in this study was superimposed onto the corresponding position of Vps4a-MIT. Then the tubulin tetramer, taken from PDB code 3du7, was superimposed onto the C-terminal helix of CHMP1a with the best one position selected out of the eight candidate positions of tubulin.

RESULTS

Structural Prediction and Sequence Analysis of kp60-NTD—Prior to structural determination, we extensively analyzed residues 1–90 of the N-terminal sequences of mouse and human kp60, which represent the sequences preceding the AAA domains, by both bioinformatics and biophysical methods (17). In brief, we found that these regions are genetically conserved only within a single subfamily of type I AAA-ATPase, corresponding to kp60 orthologs (Fig. 1*B*). Members of this family are found in mammals, other vertebrates, plants, insects, urchins, and nematodes, but not in yeasts or bacteria. It should be noted that some archaeal kp60s (*e.g.* gi: 13814089 and 223478990) that lack this N-terminal region are less well related

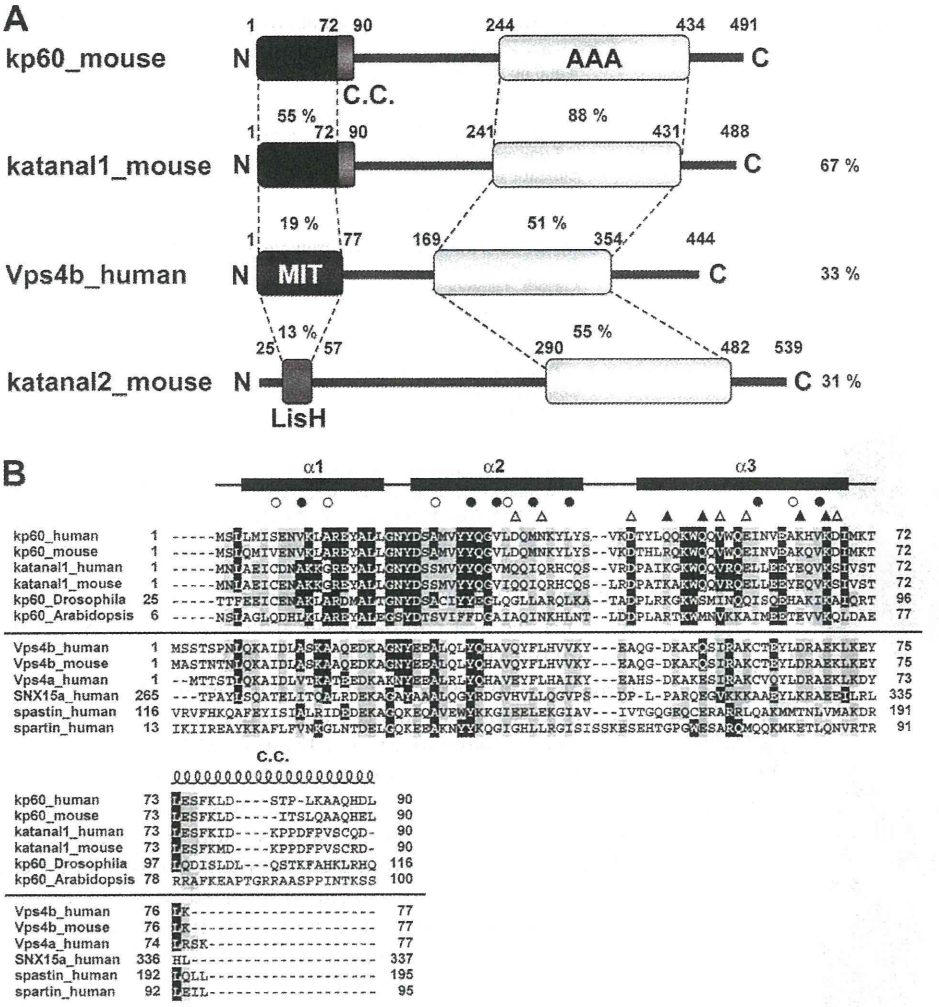

FIGURE 1. **Domain architectures and multiple sequence alignment of kp60s and proteins containing MIT domains.** *A*, domain architectures of mouse kp60, katanal1 and -2, and human Vps4b. The amino acid identities of each domain and full-length proteins between kp60 and other proteins are indicated. *C.C.*, coiled-coil; *MIT*, MIT domain; *LisH*, LIS1 homology domain; *AAA*, AAA domain. *B*, multiple sequence alignment of kp60-NTDs and related proteins with secondary structure elements of kp60-NTD. The secondary structure elements are shown at the *top* of the figure. The α-helices (α1–3) are represented as *thick lines* and the C.C. region as a coil. *Filled* and *open circles above* the alignments indicate well conserved and less conserved core residues, respectively (see Fig. 2*A*). *Triangles* indicate residues substituted with Ala for examining tubulin binding. (*Filled triangle*, involved in tubulin binding; *open triangle*, not involved.) Protein names and UniProtKB accession numbers are as follows: kp60 human (O75449); kp60 mouse (Q9WV86); kp60 *Drosophila* (Q9VN89); kp60 *Arabidopsis* (Q9SEX2); katanal1 human (Q9BW62); katanal1 mouse (Q8K0T4); Vps4b human (O75351); Vps4b mouse (P46467); Vps4a human (Q9UN37); SNX15a human (Q9NRS6); spartin human (Q8N0X7); and spastin human (Q9UBP0). The sequence alignment was generated by ClustalX (62).

to other kp60s, although a strong relationship is found for Vps4 orthologs. Thus, these archaeal kp60s may be better annotated as Vps4 homologs (35).

Focusing upon the AAA-ATPase domain and analyzing the domain level phylogenetic tree, the type I AAA-ATPases, including kp60, spastin, and Vps4, form a single cluster (7, 36). The kp60 orthologs with a conserved N-terminal region form a small subfamily, which is different from the Vps4 subfamily (supplemental Fig. 1). In some mammalian genomes (*e.g.* mouse, rat, and human), kp60-like A1s (katanal1s) are also conserved (Fig. 1). Katanal1s are very similar kp60 paralogs (~67% sequence identity over the entire chain). Moreover, this region (residues 1–90) can be further divided into two parts as follows: a well conserved core region (residues 1–72) and the following less-conserved region (~18 residues). The latter was a putative coiled-coil region, and the N-terminal region (residues 1–90) may form a dimer (17), whereas the first 72 residues behaved as an ideal "NMR ready" monomer. We call this region (residues 1–72) the core N-terminal domain (denoted kp60-NTD) and used it for further analysis.

Structure of kp60-NTD—kp60-NTD was analyzed by standard solution NMR techniques. All of the backbone and 96% of the nonexchangeable protons of the side chain signals were assigned. An ensemble of 20 structures with low CYANA target functions (Fig. 2*A*) was generated from 1723 experimental NMR constraints. These 20 structures satisfy the experimental constraints very well (Table 1). The stereochemical quality of the ensemble members is good, with all backbone ϕ/ψ angles occupying the most favored or additionally allowed regions of the Ramachandran plot (Table 1; supplemental Fig. 2). Excluding the disordered regions, *i.e.* the N-terminal region (residues 1–3 plus the preceding extra six residues of the tag) and the C-terminal region (residues 69–72), the r.m.s.d. values were 0.33 Å for backbone heavy atoms and 0.83 Å for all heavy atoms.

As shown in Fig. 2*B*, kp60-NTD is organized into antiparallel three-helix bundle that consists of helix 1 (4–19), helix 2 (23–41), and helix 3 (46–69). The secondary structure is shown in Fig. 1*B* along with its amino acid sequence. Helices 1 and 2 are connected by a very tight three-residue turn, whereas helices 2 and 3 are connected by a more flexible four-residue loop. Helices 2 and 3 are longer than helix 1, thereby exposing a large protrusion formed by helix 2 C terminus and helix 3 N terminus. These three helices are packed against one another nearly in parallel. The packing angles between the helices are similar as follows: 19.3° between 1 and 2, 21.1° between 2 and 3, and 26.1° between 1 and 3. Interhelical contacts mainly include hydrophobic side chain-side chain interactions. Core residues employed in these contacts are shown in Fig. 2*A* as well as in Fig. 1*B*. A total of 12 nonpolar contacts between helices 1 and 2, 17 between helices 2 and 3, and 5 between helices 1 and 3 were observed. The spatial arrangement of these three helices is nearly symmetric. The interhelical distances between helices 1

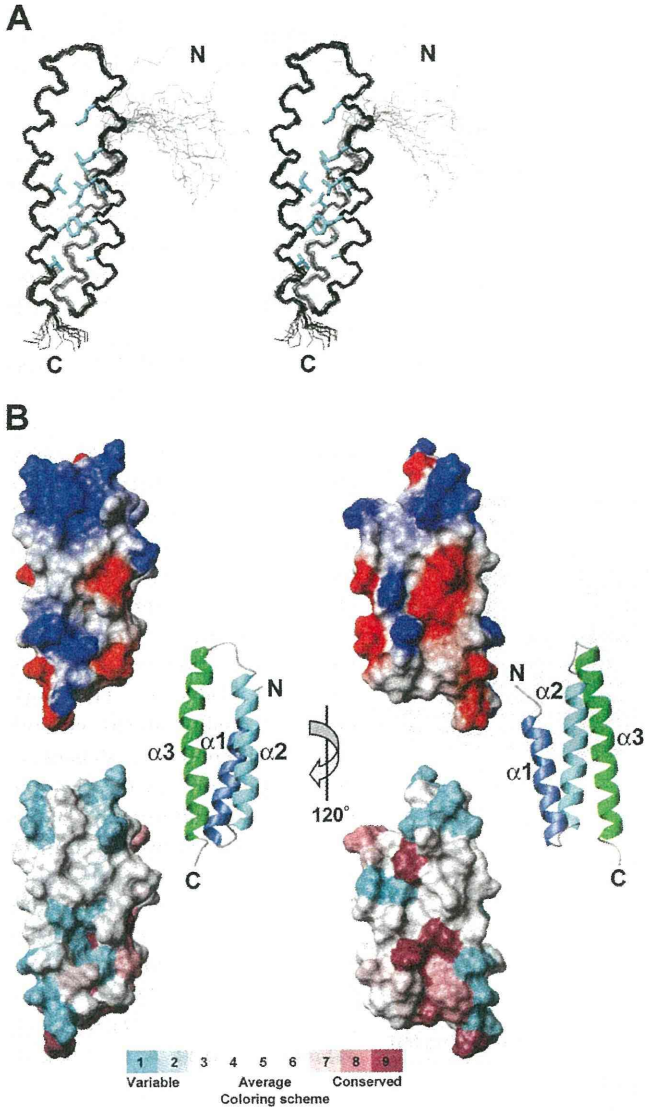

FIGURE 2. **Solution structure of kp60-NTD.** *A*, stereo view of the best fit superposition of the 20 structures with lowest target functions. Side chains of buried residues with solvent accessibility less than 10% are shown (*cyan*). *B*, *top*, electrostatic surface potential mapped onto a van der Waals surface diagram. The color scale ranges between -20 k_BT (*red*) to $+20$ k_BT (*blue*), where k_B is Boltzmann's constant and T is temperature. *Bottom*, sequence conservation among the kp60-NTDs is mapped on the surface. Conservative and variable residues are colored *purple* and *cyan*, respectively. The color codes were produced by ConSurf (63). Ribbon diagrams of the kp60-NTDs are shown in the *middle*. The surface composed of helices 2 and 3 is shown as the front view (*left*) and the rear view (*right*).

and 2 (5.0 Å) and helices 2 and 3 (5.5 Å) were shorter than that between helices 1 and 3 (6.5 Å). We found no obvious crevices or pockets on the surface of kp60-NTD. The kp60-NTD surface is highly charged (Fig. 2*B*).

Structural Similarities of kp60-NTD with MIT Domains and Other Tetratricopeptide Repeat Proteins—When the structure of kp60-NTD was subjected to DALI search (37), several MIT domains were first retrieved with Z-scores higher than 7.0, including NRBF-2 (PDB code 2crb, Z-score of 9.6, and r.m.s.d. of 1.6 Å), Vps4b (PDB code 1wr0, Z-score of 8.9, and r.m.s.d. of 2.7 Å), Vta1 (PDB code 2rkk, Z-score of 7.4, and r.m.s.d. of 2.4 Å), spastin (PDB code 3eab, Z-score of 7.2, and r.m.s.d. of 2.2 Å),

TABLE 1
Experimental restraints and statistics for 20 structures of kp60-NTD

Distance restraints	
Total no. of restraints	1723
Intraresidue	Unused
Sequential restraints ($\|i-j\|=1$)	831
Medium range restraints ($1<\|i-j\|\leq 4$)	462
Long range restraints ($\|i-j\|>4$)	304
Dihedral angle restraints	126
$\phi/\psi/\chi$	63/63/0
Hydrogen bond restraints	0
Statistics used for and obtained from the structure calculations	
Final Statistics (20/100)	
Cutoffs, distance (0.3 Å) and angle (3.0°)	
Maximum target function	0.06
Maximum violations	
Distance violation	0.21 Å
Angle violation	9.15°
Coordinate precision (residues 4–68)	
Backbone r.m.s.d.	0.33 Å
Heavy atom r.m.s.d.	0.83 Å
Ramachandran plot statistics (%) (all residues)	
Residues in most favored regions	92.2
Residues in additionally allowed regions	7.1
Residues in generously allowed regions	0.1
Residues in disallowed regions	0.0

and spartin (PDB code 2dl1, Z-score of 7.1, and r.m.s.d. of 2.4 Å). Thus, we first compared the structure of kp60-NTD with those of the MIT domains. Fig. 3 shows the structural comparisons between kp60-NTD and each of the MIT domains along with their sequence identity and structural fitness. Despite a low sequence similarity (10–19%), the kp60-NTD fold resembles those of the MIT domains, as shown by backbone r.m.s.d. of 2.2–2.7 Å for more than 67 residues from the secondary structural regions. Among these, spastin is the product of SPG4, which is mutated in the most common form of hereditary spastic paraplegia (4), and is involved with MT maintenance in axons (38, 39). Thus, the MIT domain of spastin is one of the closest homolog of kp60-NTD with regard to its physiological relevance to MT severing.

After comparing the structures in detail, all the helices were well superimposed, although the loop between helices 2 and 3 was not (Fig. 3*E*). The structures of the kp60 tubulin-binding site, kp60-NTD, and the MIT domain were strikingly similar, although their sequence similarity was very low (~19%). Thus, kp60-NTD is classified as a variant MIT domain. Because some of the MIT domains (*e.g.* spastin and spartin) are considered to bind microtubule (and/or tubulin), this structural similarity is not surprising.

One of the most characteristic features of the MIT domain is its unique hydrophobic core formed by conserved Ala residues, referred to as the "Ala zipper" (40, 41). These are thus identified as the key residues for the MIT domain signature (Ala-Xaa$_6$-Ala-Xaa$_{11}$-Ala-Xaa$_6$-Ala). These conserved Ala residues are present along the buried surfaces of helices 1–3 facing each other, thereby forming a hydrophobic core. In kp60 and its closely related homologs, these key Ala residues are only partly conserved. For example, Ile-6 and Val-32 in mouse kp60-NTD correspond to the zipper-forming Ala residues (Ala-9 and Ala-35) in the human Vps4a-MIT domain. Although the MIT domain signature is not conserved in kp60-NTD, this domain is obviously a close variant of the MIT domain. This imperfect conservation of the MIT-domain signature may explain why methods such as PSI-BLAST (18) and HMMER (19) could not

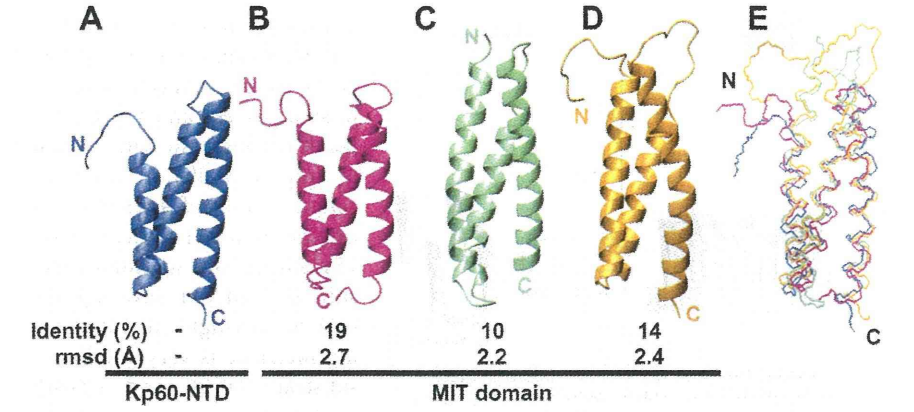

FIGURE 3. **Structural comparisons of kp60-NTD with MIT domains.** Ribbon diagrams of the proteins are as follows: *A*, kp60 (PDB code 2rpa); *B*, Vps4b (PDB code 1wr0); *C*, spastin (PDB code 3eab); *D*, spartin (PDB code 2dl1). Identity (*top*, %) and r.m.s.d. (*bottom*, Å) between kp60-NTD and the MIT domains are also presented. *E*, superposition of kp60-NTD (*blue*), Vps4b-MIT (*magenta*), spastin-MIT (*pale green*), and spartin-MIT (*orange*).

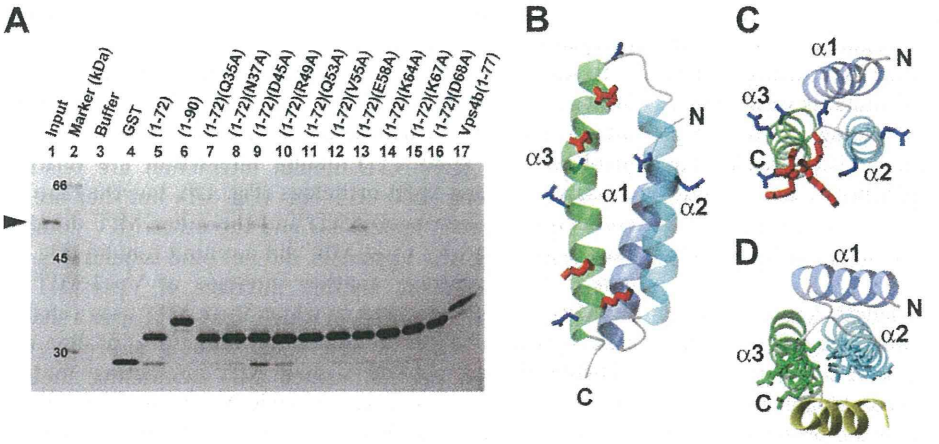

FIGURE 4. **Interactions of kp60-NTD with tubulin.** *A*, pulldown assays of tubulin with GST-tagged kp60-NTDs of wild type and Ala mutants and Vps4b-MIT *in vitro*. Tubulin was used as the input. Molecular size is shown in *lane 2*. Only the buffer and the GST tag used as negative controls are shown in *lanes 3* and *4*. Recombinant proteins used for pulldown are indicated at the top of the gel. SDS-PAGE was silver-stained. *B* and *C*, side and top views of the ribbon diagram of kp60-NTD, respectively. Side chains of residues that were substituted with Ala are shown. In the pulldown assay, residues that were affected and unaffected by Ala mutations for tubulin binding are colored *red* and *blue*, respectively. *D*, top view of the ribbon diagram of the complex between Vps4-MIT and CHMP1a (*yellow*) (PDB code 2jq9). Side chains of the residues interacting between Vps4 and CHMP1a are indicated.

predict the structural similarity between kp60-NTD and the MIT domain. In the DALI search, we also found other proteins containing either twisted α-helical hairpins or tetratricopeptide repeat motifs with Z-scores higher than 5.0. For example, partial structures of glycine-tRNA synthetase α-chain (PDB code 1j5w, Z-score of 8.7, and r.m.s.d. of 2.2 Å), 14-3-3 protein Tau (PDB code 2btp, Z-score of 8.2, and r.m.s.d. of 2.4 Å), cyclophilin 40 (PDB code 1ihg, Z-score of 8.1, and r.m.s.d. of 2.7 Å), α-E-catenin (PDB code 1l7c, Z-score of 7.9, and r.m.s.d. of 2.0 Å), fkbp52 (PDB code 1p5q, Z-score of 7.5, and r.m.s.d. of 3.0 Å), invertase inhibitor Nt-CIF (PDB code 1rj1, Z-score of 6.3, and r.m.s.d. of 2.1 Å), and Hop (PDB code 1elr, Z-score of 5.2, and r.m.s.d. of 3.7 Å) were shown to resemble kp60-NTD (data not shown).

Tubulin Binding by kp60-NTDs—To examine the molecular function of kp60-NTD as an MT binding domain, we performed *in vitro* MT binding assays using polymerized MTs. Contrary to our expectation, we found that the amount of kp60-NTD co-sedimented with MTs was very low, at the limit of detectability (supplemental Fig. 3) (data not shown). However, kp60-NTD co-sedimented with medium size MTs (supplemental Fig. 3*D*). These results suggested that kp60-NTD might bind to oligomeric tubulin and/or MT fragments rather than enormous polymerized MTs. Thus, we did a pulldown assay using GST-tagged kp60-NTD with unpolymerized tubulin. *In vitro* tubulin binding activity of kp60-NTD was observed (Fig. 4*A*, *lane 5*).

This tubulin binding activity varied with the length of the N-terminal domain. kp60-NTD (residues 1–72) binds tubulin, whereas kp60-NTD (residues 1–90) does not (Fig. 4*A*, *lane 6*). In our previous report, we showed that kp60-NTD (residues 1–90) formed a dimer using the coiled-coil region (residues 73–90) (17). Thus, dimer formation may hide the interface of kp60-NTD from tubulin. In addition, we found that the Vps4b-MIT domain (residues 1–77) did not bind tubulin (Fig. 4*A*, *lane 17*). Thus, the observed tubulin binding activity is specific for kp60-NTD.

Tubulin-binding Site of kp60-NTD—To determine the interfacial residues on kp60-NTD involved with tubulin recognition, we carried out mutagenesis experiments. Prior to these experiments, we attempted to identify the tubulin-interacting residues on kp60-NTD by NMR titration experiments and failed. We observed unexpected severe signal broadening even at very low tubulin concentration, which made further NMR analysis difficult (data not shown). Then, 10 residues from kp60-NTD (Gln-35, Asn-37, Asp-45, Arg-49, Gln-53, Val-55, Glu-58, Lys-64, Lys-67, and Asp-68) were selected, and each was substituted with Ala. These residues were carefully selected from the surface residues located on helices 2 and 3. The binding activities of mutants were examined by pulldown experiments (Fig. 4*A*, *lanes 7–16*).

The most significant effects were observed in mutations of residues on helix 3 as follows: Arg-49, Gln-53, Lys-64, and Lys-67. All of these side chains are hydrophilic and are exposed to the surface composed of helices 2 and 3 (Fig. 4, *B* and *C*). In addition, three of the four key residues are positively charged, suggesting an electrostatic interaction between kp60-NTD and tubulin. These residues were not conserved in the Vps4b-MIT domain as well as in the other MIT domains, such as spastin and spartin (Fig. 1*B*). This result is partially consistent with the

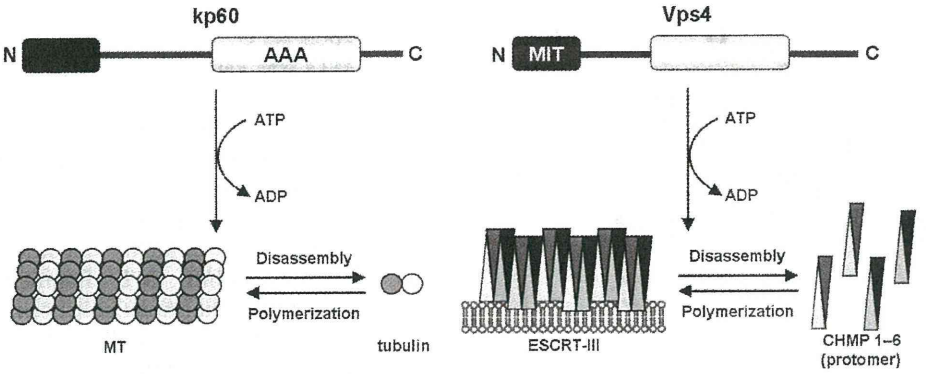

FIGURE 5. **Schematic diagram of architecture and molecular function similarities between kp60 and Vps4.** kp60 catalyzes the disassembly of MT via N-terminal domain binding, which results in MT severing. Vps4 catalyzes the release of the ESCRT-III protomer via the MIT domain binding, which results in endosomal membrane invagination. For both biological events, the N-terminal domains serve as adaptors for the polymeric macromolecules, thereby disassembling either the cytoskeleton or the membrane skeleton in an ATP-dependent manner.

inability of Vps4b-MIT to bind tubulin (Fig. 4*A*, *lane 17*). Because spastin and spartin can bind or regulate MTs (42, 43), this might indicate that these proteins bind MTs using regions other than the MIT domains. In contrast, mutants V55A, E58A, and D68A retained substantial tubulin binding activities (Fig. 4*A*, *lanes 12, 13,* and *16*). These residues are also on helix 3, but are exposed to the surface composed of helices 1 and 3 or outside of helix 3 (Fig. 4, *B* and *C*). Similarly, residues in helix 2 (Gln-35 and Asn-37) and loop 2 (Asp-45) were not involved in tubulin binding (Fig. 4*A*, *lanes 7–9*).

We further examined whether full-length kp60s with or without mutation in the N-terminal domain bind tubulin. We generated GST-tagged full-length kp60 in *E. coli*. Prior to the binding assay, we confirmed that the recombinant full-length kp60s had ATPase activity, according to the protocol in the recent paper (supplemental Fig. 4*A*) (16). We then performed pulldown experiments using mutants R49A and K67A of full-length kp60. The full-length kp60 (wild type) bound tubulin, whereas the mutants lacked tubulin binding activities, as expected by the results of kp60-NTDs (supplemental Fig. 4*B*; Fig. 4*A*).

DISCUSSION

Structural and Functional Comparisons with Other Tubulin Binding Domains—In this study, we have determined the structure of a novel tubulin binding domain derived from the conserved region of kp60, which was classified as a variant MIT domain. To our knowledge, this is the first experimental evidence for the direct interaction between an isolated MIT domain and tubulin.

To date, structures of many MT and/or tubulin binding domains have been determined (supplemental Fig. 5) (44–49). Interestingly, all-α-helical protein domains are dominant in these with solved structures, which might be advantageous for interactions with MT and/or tubulin. In the MT structure, the only accessible surface of tubulin includes helices 11 and 12 and the C-terminal tail (49–51). Thus, for one of tubulin recognition, helix-helix interactions of tubulin binding domains are suggested, although there are many structures of the known MT-interacting proteins left unsolved.

Structural and Functional Similarities to Vps4—We identified the tubulin-binding interface of kp60-NTD, which is on the surface comprising helices 2 and 3 (Fig. 4*B*). This result is consistent with the studies by Stoppin-Mellet, in which a truncation mutant of *Arabidopsis* kp60 (*At*KSS) that lacked the N-terminal 15 residues corresponding to helix 1 still retained MT severing activity (16). Surprisingly, the tubulin binding interface is very similar to the substrate (Vps2 and CHMP1a)-binding interfaces of the MIT domains of Vps4 (Fig. 4, *C* and *D*) (35, 52, 53). In other words, the common substrate-binding interfaces appear to be preserved between MT severing and membrane skeletal reorganization.

In studies of Vps4-MIT complexed with C-terminal regions of Vps2 or CHMP1a, the MIT domains use helices 2 and 3 as the interface for the α-helical peptides (35, 52). The residues involved with kp60-NTD-tubulin interaction are relatively conserved among kp60 orthologs (Fig. 1*B*), but they are not conserved between kp60-NTD and the other MIT domains, thus explaining why Vps4-MIT did not bind tubulin (Fig. 4*A*, *lane 17*). In contrast, another interface of Vps4-MIT for CHMPs has been reported, in which Vps4-MIT uses a shallow cleft between helices 1 and 3 for binding a proline-rich, CHMP6-derived peptide named MIT-interacting motif 2 (MIM2) (53). In the structure of kp60-NTD, there was no correspondence between helices 1 and 3, as the interhelical distance was substantially narrower (6.5 Å) than that of Vps4-MIT. We do not rule out the possibility that the interface composed of helices 1–3 serves as the binding site of other factors, such as katanin p80 and NDEL1 (54), both of which regulate the subcellular localization of kp60.

Conserved Macromolecular Disassembling Mechanisms between Vps4 and Kp60—Our findings indicate that the molecular architectures of kp60 and Vps4 are very similar in the following points: domain organization, structures of the N-terminal domains, and the relative locations of the interfaces for target proteins. Here, we propose some common features of the molecular mechanisms in different biological processes, MT severing and late endosomal luminal membrane budding, driven by kp60 and Vps4, respectively.

First, both the enzymes disassemble polymeric macromolecular complexes known as cytoskeleton and membrane skeleton. Second, these enzymes release protomers from macromolecular complexes (MT and ESCRT-III) in the cytoplasm depending on ATP hydrolysis. Finally, their N-terminal domains serve as adaptors to the protomers. The similarities of these mechanisms are illustrated in Fig. 5.

The ESCRT-III complex is composed of self-associating coiled-coil proteins (CHMP1–6), which form filamentous circular structures on the membrane surface (55). When Vps4 interacts with ESCRT-III filaments, it pulls out CHMP pro-

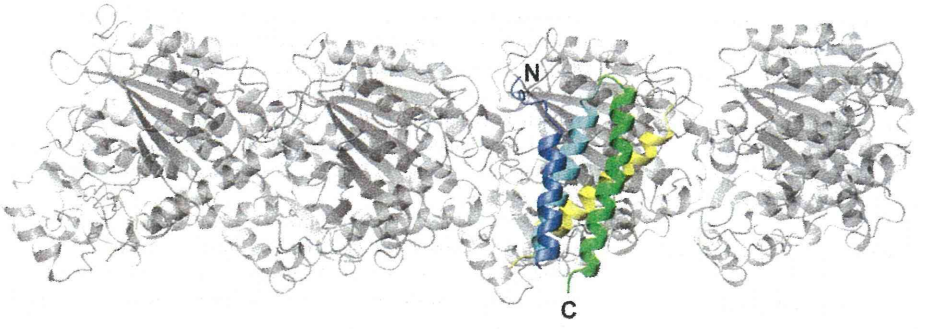

FIGURE 6. **Model of α-tubulin binding with kp60-NTD.** Ribbon diagram of a model complex between kp60-NTD and a tubulin tetramer (*gray*) is shown. α-Tubulin helix 12, a putative interface of kp60-NTD, is colored *yellow*.

tomers from the filamentous circular structure. The residual filaments of ESCRT-III then reorganize into a smaller circular structure by self-association. Vps4 continues to pull protomers away, and the circular structure shrinks into a smaller wheel. Finally, this downsizing of the ESCRT-III circle results in membrane budding with concomitant alterations of the membrane structure. This model is known as the "concentric circle model" (56).

We propose that the early stage of MT severing might have a similar mechanism. kp60 pulls a tubulin α/β-dimer away from MT in an ATP-dependent manner. However, contrary to the ESCRT-III polymer, polymerization of tubulin dimers is restricted to the plus end of MT as well as to the GTP form of tubulin, whereas polymerization at the minus end is extremely slow (reviewed in Refs. 1, 57). It is expected that once tubulin is pulled away by kp60, it can no longer fill the gap on MT. If two or more tubulin dimers are pulled away from this gap, then MT may start severing, resulting in a catastrophe. The structural similarities between kp60 and Vps4 revealed in this study encourage us to propose a model for the molecular mechanism of MT severing.

Model for kp60-NTD Binding to Tubulin Oligomer—To assess the detailed mechanism of MT severing, we constructed a model for the complex between kp60-NTD and a tubulin tetramer (Fig. 6). Our study is confined to the interface of the kp60 N-terminal adaptor domain to its tubulin substrate, as we did not identify the kp60-binding site on tubulin. Nevertheless, numerous literature resources provide a basis for model construction as follows. As discussed previously, the major candidates of the structural elements of tubulin that are accessible from outside MT are helices 11 and 12 (49–51). Next, the similarity between the interfaces of kp60-NTD with tubulin and that of Vps4-MIT with CHMP1a suggests that a helix on tubulin, which is similar to the CHMP1a helix (residues 115–127) bound to Vps4-MIT (52), may serve as the binding site of kp60. Taking all the information into account, we propose a model for the tubulin + kp60-NTD complex (Fig. 6).

While constructing the model, the following points were hypothesized: (i) one of the last helices (helix 11 or 12) makes contact with kp60-NTD at its helix 2/3 interface; (ii) the relative position and orientation between kp60-NTD and one of the tubulin helices mimic those between Vps4-MIT and the CHMP1a helix; (iii) steric crash between kp60-NTD and tubulin should be avoided; and (iv) charge-charge interactions between kp60-NTD and the tubulin helix should be maximized.

As a result, we found the following four candidate positions on tubulin C-terminal helices for kp60-NTD binding: (i) helix 11 (residues 386–396); (ii) helix 11 (residues 390–400); (iii) helix 12 (residues 420–430); and (iv) helix 12 (residues 423–433). All these positions are present on both tubulin-α and tubulin-β. Finally, by assessing complementarity of charge interactions in the model, the final model was selected out of the eight candidate models. Its helix 12 (residues 420–430) of tubulin α3 binds with kp60-NTD by occupying the corresponding position of CHMP1a (residues 115–127) that binds Vps4-MIT (PDB code 2jq9) (Fig. 6; supplemental Fig. 6) (52).

Alternatively, we generated the model of kp60-NTD + tubulin tetramer complex based on the complex between spastin-MIT with CHMP1b (PDB code 3eab) in which spastin-MIT used helices 1 and 3 as the interface to CHMP1b (supplemental Fig. 7) (58). This model is not consistent with our mutation studies (Fig. 4). Consequently, we justified the modeling of helices 2 and 3 as the tubulin-binding site. Because CHMP1b serves as an adaptor of spastin but not a substrate, this alternative model suggests that the helix 1/3 surface of kp60-NTD is a putative binding site for kp80, an adaptor of kp60 to bound MT and/or tubulin.

In the model of Fig. 6, the direction of the pore of the hexameric AAA-ATPase domain, which follows C-terminal to kp60-NTD, may approach the C-terminal tail of tubulin. We further confirmed this idea by using the model structure of full-length hexameric kp60 complexes with tubulin (supplemental Fig. 8). The location is consistent with the hypothesis that the pore of the AAA domain "sucks in" the tubulin C-terminal tail upon ATP hydrolysis (threading model) (59, 60). In fact, the literature suggests that kp60 function requires its direct interaction with the C-terminal tail of tubulin. This is based on the observation that MT severing activity was abolished when MTs were pretreated with subtilisin (8). Additional evidence regarding the MT-severing mechanism of spastin, another related AAA-ATPase, may support this idea. Spastin also recognizes and pulls the tubulin C-terminal tail as an initial binding site that is indispensable for its MT severing activity (42, 61). The hypotheses derived from our complex model require confirmation by additional experimentation.

In conclusion, the structure and key residues of kp60-NTD provide new insights into the molecular mechanisms of how the enzyme severs MT. The similarities of the molecular mechanisms as well as of the domain organizations suggest that these are evolutionally conserved among type I AAA-ATPases, kp60 and Vps4, whose cellular functions are distinct.

Acknowledgment—We thank Kaori Satomura for technical assistance.

REFERENCES

1. Desai, A., and Mitchison, T. J. (1997) *Annu. Rev. Cell Dev. Biol.* **13,** 83–117
2. Wittmann, T., Hyman, A., and Desai, A. (2001) *Nat. Cell Biol.* **3,** E28–E34
3. Zhang, D., Rogers, G. C., Buster, D. W., and Sharp, D. J. (2007) *J. Cell Biol.* **177,** 231–242
4. Hazan, J., Fonknechten, N., Mavel, D., Paternotte, C., Samson, D., Artiguenave, F., Davoine, C. S., Cruaud, C., Dürr, A., Wincker, P., Brottier, P., Cattolico, L., Barbe, V., Burgunder, J. M., Prud'homme, J. F., Brice, A., Fontaine, B., Heilig, B., and Weissenbach, J. (1999) *Nat. Genet.* **23,** 296–303
5. Errico, A., Ballabio, A., and Rugarli, E. I. (2002) *Hum. Mol. Genet.* **11,** 153–163
6. Cox, G. A., Mahaffey, C. L., Nystuen, A., Letts, V. A., and Frankel, W. N. (2000) *Nat. Genet.* **26,** 198–202
7. Frickey, T., and Lupas, A. N. (2004) *J. Struct. Biol.* **146,** 2–10
8. McNally, F. J., and Vale, R. D. (1993) *Cell* **75,** 419–429
9. Hartman, J. J., Mahr, J., McNally, K., Okawa, K., Iwamatsu, A., Thomas, S., Cheesman, S., Heuser, J., Vale, R. D., and McNally, F. J. (1998) *Cell* **93,** 277–287
10. McNally, K. P., Bazirgan, O. A., and McNally, F. J. (2000) *J. Cell Sci.* **113,** 1623–1633
11. McNally, F. J., Okawa, K., Iwamatsu, A., and Vale, R. D. (1996) *J. Cell Sci.* **109,** 561–567
12. McNally, F. J., and Thomas, S. (1998) *Mol. Biol. Cell* **9,** 1847–1861
13. Hartman, J. J., and Vale, R. D. (1999) *Science* **286,** 782–785
14. Lupas, A. N., and Martin, J. (2002) *Curr. Opin. Struct. Biol.* **12,** 746–753
15. Ogura, T., and Wilkinson, A. J. (2001) *Genes Cells* **6,** 575–597
16. Stoppin-Mellet, V., Gaillard, J., Timmers, T., Neumann, E., Conway, J., and Vantard, M. (2007) *Plant Physiol. Biochem.* **45,** 867–877
17. Iwaya, N., Goda, N., Unzai, S., Fujiwara, K., Tanaka, T., Tomii, K., Tochio, H., Shirakawa, M., and Hiroaki, H. (2007) *J. Biomol. NMR* **37,** 53–63
18. Altschul, S. F., Madden, T. L., Schäffer, A. A., Zhang, J., Zhang, Z., Miller, W., and Lipman, D. J. (1997) *Nucleic Acids Res.* **25,** 3389–3402
19. Bateman, A., Birney, E., Cerruti, L., Durbin, R., Etwiller, L., Eddy, S. R., Griffiths-Jones, S., Howe, K. L., Marshall, M., and Sonnhammer, E. L. (2002) *Nucleic Acids Res.* **30,** 276–280
20. Bateman, A., Coin, L., Durbin, R., Finn, R. D., Hollich, V., Griffiths-Jones, S., Khanna, A., Marshall, M., Moxon, S., Sonnhammer, E. L., Studholme, D. J., Yeats, C., and Eddy, S. R. (2004) *Nucleic Acids Res.* **32,** D138–D141
21. Letunic, I., Copley, R. R., Schmidt, S., Ciccarelli, F. D., Doerks, T., Schultz, J., Ponting, C. P., and Bork, P. (2004) *Nucleic Acids Res.* **32,** D142–D144
22. Tomii, K., and Akiyama, Y. (2004) *Bioinformatics* **20,** 594–595
23. Shi, J., Blundell, T. L., and Mizuguchi, K. (2001) *J. Mol. Biol.* **310,** 243–257
24. Ciccarelli, F. D., Proukakis, C., Patel, H., Cross, H., Azam, S., Patton, M. A., Bork, P., and Crosby, A. H. (2003) *Genomics* **81,** 437–441
25. Goda, N., Tenno, T., Takasu, H., Hiroaki, H., and Shirakawa, M. (2004) *Protein Sci.* **13,** 652–658
26. Yamazaki, T., Lee, W., Arrowsmith, C. H., Muhandiram, D. R., and Kay, L. E. (1994) *J. Am. Chem. Soc.* **116,** 11655–11666
27. Cavanagh, J., Fairbrother, W. J., Palmer, A. G., 3rd, Rance, M., and Skelton, N. J. (2007) *Protein NMR Spectroscopy: Principles and Practice,* 2nd Ed., pp. 535–673, Academic Press, San Diego
28. Delaglio, F., Grzesiek, S., Vuister, G. W., Zhu, G., Pfeifer, J., and Bax, A. (1995) *J. Biomol. NMR* **6,** 277–293
29. Goddard, T. D., and Kneller, D. G. (2004) *SPARKY,* Version 3, University of California, San Francisco
30. Herrmann, T., Güntert, P., and Wüthrich, K. (2002) *J. Mol. Biol.* **319,** 209–227
31. Guntert, P. (2003) *Prog. Nucleic Magn. Reson. Spect.* **43,** 105–125
32. Cornilescu, G., Delaglio, F., and Bax, A. (1999) *J. Biomol. NMR* **13,** 289–302
33. Koradi, R., Billeter, M., and Wuthrich, K. (1996) *J. Mol. Graph.* **14,** 29–32
34. Laskowski, R. A., Rullmannn, J. A., MacArthur, M. W., Kaptein, R., and Thornton, J. M. (1996) *J. Biomol. NMR* **8,** 477–486
35. Obita, T., Saksena, S., Ghazi-Tabatabai, S., Gill, D. J., Perisic, O., Emr, S. D., and Williams, R. L. (2007) *Nature* **449,** 735–739
36. Fröhlich, K. U. (2001) *J. Cell Sci.* **114,** 1601–1602
37. Holm, L., and Sander, C. (1997) *Nucleic Acids Res.* **25,** 231–234
38. Sherwood, N. T., Sun, Q., Xue, M., Zhang, B., and Zinn, K. (2004) *PLoS. Biol.* **2,** e429
39. Evans, K. J., Gomes, E. R., Reisenweber, S. M., Gundersen, G. G., and Lauring, B. P. (2005) *J. Cell Biol.* **168,** 599–606
40. Takasu, H., Jee, J. G., Ohno, A., Goda, N., Fujiwara, K., Tochio, H., Shirakawa, M., and Hiroaki, H. (2005) *Biochem. Biophys. Res. Commun.* **334,** 460–465
41. Scott, A., Gaspar, J., Stuchell-Brereton, M. D., Alam, S. L., Skalicky, J. J., and Sundquist, W. I. (2005) *Proc. Natl. Acad. Sci. U.S.A.* **102,** 13813–13818
42. White, S. R., Evans, K. J., Lary, J., Cole, J. L., and Lauring, B. (2007) *J. Cell Biol.* **176,** 995–1005
43. Patel, H., Cross, H., Proukakis, C., Hershberger, R., Bork, P., Ciccarelli, F. D., Patton, M. A., McKusick, V. A., and Crosby, A. H. (2002) *Nat. Genet.* **31,** 347–348
44. Ravelli, R. B., Gigant, B., Curmi, P. A., Jourdain, I., Lachkar, S., Sobel, A., and Knossow, M. (2004) *Nature* **428,** 198–202
45. Slep, K. C., and Vale, R. D. (2007) *Mol. Cell* **27,** 976–991
46. Mishima, M., Maesaki, R., Kasa, M., Watanabe, T., Fukata, M., Kaibuchi, K., and Hakoshima, T. (2007) *Proc. Natl. Acad. Sci. U.S.A.* **104,** 10346–10351
47. Guasch, A., Aloria, K., Pérez, R., Avila, J., Zabala, J. C., and Coll, M. (2002) *J. Mol. Biol.* **318,** 1139–1149
48. Carter, A. P., Garbarino, J. E., Wilson-Kubalek, E. M., Shipley, W. E., Cho, C., Milligan, R. A., Vale, R. D., and Gibbons, I. R. (2008) *Science* **322,** 1691–1695
49. Kikkawa, M., and Hirokawa, N. (2006) *EMBO J.* **25,** 4187–4194
50. Nogales, E., Wolf, S. G., and Downing, K. H. (1998) *Nature* **391,** 199–203
51. Bodey, A. J., Kikkawa, M., and Moores, C. A. (2009) *J. Mol. Biol.* **388,** 218–224
52. Stuchell-Brereton, M. D., Skalicky, J. J., Kieffer, C., Karren, M. A., Ghaffarian, S., and Sundquist, W. I. (2007) *Nature* **449,** 740–744
53. Kieffer, C., Skalicky, J. J., Morita, E., De Domenico, I., Ward, D. M., Kaplan, J., and Sundquist, W. I. (2008) *Dev. Cell* **15,** 62–73
54. Toyo-Oka, K., Sasaki, S., Yano, Y., Mori, D., Kobayashi, T., Toyoshima, Y. Y., Tokuoka, S. M., Ishii, S., Shimizu, T., Muramatsu, M., Hiraiwa, N., Yoshiki, A., Wynshaw-Boris, A., and Hirotsune, S. (2005) *Hum. Mol. Genet.* **14,** 3113–3128
55. Hanson, P. I., Roth, R., Lin, Y., and Heuser, J. E. (2008) *J. Cell Biol.* **180,** 389–402
56. Nickerson, D. P., Russell, M. R., and Odorizzi, G. (2007) *EMBO Rep.* **8,** 644–650
57. Howard, J., and Hyman, A. A. (2003) *Nature* **422,** 753–758
58. Yang, D., Rismanchi, N., Renvoisé, B., Lippincott-Schwartz, J., Blackstone, C., and Hurley, J. H. (2008) *Nat. Struct. Mol. Biol.* **15,** 1278–1286
59. Sauer, R. T., Bolon, D. N., Burton, B. M., Burton, R. E., Flynn, J. M., Grant, R. A., Hersch, G. L., Joshi, S. A., Kenniston, J. A., Levchenko, I., Neher, S. B., Oakes, E. S., Siddiqui, S. M., Wah, D. A., and Baker, T. A. (2004) *Cell* **119,** 9–18
60. Lum, R., Tkach, J. M., Vierling, E., and Glover, J. R. (2004) *J. Biol. Chem.* **279,** 29139–29146
61. Roll-Mecak, A., and Vale, R. D. (2008) *Nature* **451,** 363–367
62. Thompson, J. D., Gibson, T. J., Plewniak, F., Jeanmougin, F., and Higgins, D. G. (1997) *Nucleic Acids Res.* **25,** 4876–4882
63. Armon, A., Graur, D., and Ben-Tal, N. (2001) *J. Mol. Biol.* **307,** 447–463

Supplementary materials for

A COMMON SUBSTRATE RECOGNITION MODE CONSERVED BETWEEN KATANIN P60 AND VPS4 GOVERNS MICROTUBULE SEVERING AND MEMBRANE SKELETON REORGANIZATION *

Naoko Iwaya[1,2,3], Yohta Kuwahara[2,3,4], Yoshie Fujiwara[2,5], Natsuko Goda[2,4], Takeshi Tenno[2,4], Kohei Akiyama[3], Shogo Mase[2,4], Hidehito Tochio[1], Takahisa Ikegami[6], Masahiro Shirakawa[1], Hidekazu Hiroaki[2,3,4,5]

[1]Department of Molecular Engineering, Graduate School of Engineering, Kyoto University
[2]Division of Structural Biology, Graduate School of Medicine, Kobe University, 7-5-1 Kusunokicho, Chuo, Kobe, Hyogo 650-0017, Japan
[3]Field of Supramolecular Biology, International Graduate School of Arts and Sciences, Yokohama City University
[4]Institute for Bioinformatics Research and Development (BIRD), Japan Science and Technology Corporation (JST)
[5]Global-COE (Center of Excellence) Program for Integrative Membrane Biology, Kobe University
[6]Institute of Protein Research, Osaka University

Running title: Structure of the N-terminal domain of katanin p60

Adress correspondence to : Hidekazu Hiroaki, PhD., e-mail: hiroakih@med.kobe-u.ac.jp, Phone: +81 78 382 5813 / Fax: +81 78 382 5816